the vitreous base in APROP. Further investigation also is needed to obtain long-term functional outcomes of early vitrectomy for APROP with continuous management of aphakic eyes.

References

1. International Committee for the Classification of Retinopathy of Prematurity. The International Classification of Retinopathy of Prematurity revisited. Arch Ophthalmol 2005;123:991–9.
2. Uemura Y, Tsukahara I, Nagata M, et al. Diagnostic and therapeutic criteria for retinopathy of prematurity [in Japanese]. Committee's Report Appointed by the Japanese Ministry of Health and Welfare, Tokyo, Japan: Japanese Ministry of Health and Welfare, 1974. Nippon no Ganka 1975;46:553–9.
3. Morizane H. Initial sign and clinical course of the most severe form of acute proliferative retrolental fibroplasia (type II) [in Japanese]. Nippon Ganka Gakkai Zasshi 1976;80:54–61.
4. Vinekar A, Trese MT, Capone A Jr, Photographic Screening for Retinopathy of Prematurity (PHOTO-ROP) Cooperative Group. Evolution of retinal detachment in posterior retinopathy of prematurity: impact on treatment approach. Am J Ophthalmol 2008;145:548–55.
5. Azuma N, Ishikawa K, Hama Y, et al. Early vitreous surgery for aggressive posterior retinopathy of prematurity. Am J Ophthalmol 2006;142:636–43.
6. Micelli Ferrari T, Furino C, Lorusso VV, et al. Three-port lens-sparing vitrectomy for aggressive posterior retinopathy of prematurity: early surgery before tractional retinal detachment appearance. Eur J Ophthalmol 2007;17:785–9.
7. Flynn JT, Cassady J, Essner D, et al. Fluorescein angiography in retrolental fibroplasia: experience from 1969–1977. Ophthalmology 1979;86:1700–23.
8. Ng EY, Lanigan B, O'Keefe M. Fundus fluorescein angiography in the screening for and management of retinopathy of prematurity. J Pediatr Ophthalmol Strabismus 2006;43:85–90.
9. Azad R, Chandra P, Khan MA, Darswal A. Role of intravenous fluorescein angiography in early detection and regression of retinopathy of prematurity. J Pediatr Ophthalmol Strabismus 2008;45:36–9.
10. Hinz BJ, de Juan E Jr, Repka MX. Scleral buckling surgery for active stage 4A retinopathy of prematurity. Ophthalmology 1998;105:1827–30.
11. Trese MT. Scleral buckling for retinopathy of prematurity. Ophthalmology 1994;101:23–6.
12. Yamashita H, Hori S, Yamamoto T. Effect of traction on the vasculature of chorioallantoic membranes of chick embryos. Invest Ophthalmol Vis Sci 1989;30:778–82.
13. Wilkinson-Berka JL, Jones D, Taylor G, et al. SB-267268, a nonpeptidic antagonist of alpha(v)beta3 and alpha(v)beta5 integrins, reduced angiogenesis and VEGF expression in a mouse model of retinopathy of prematurity. Invest Ophthalmol Vis Sci 2006;47:1600–5.
14. Albinsson S, Hellstrand P. Integration of signal pathways for stretch-dependent growth and differentiation in vascular smooth muscle. Am J Physiol Cell Physiol 2007;293:C772–82.
15. Favard C, Guyot-Argenton C, Assouline M, et al. Full panretinal photocoagulation and early vitrectomy improve prognosis of florid diabetic retinopathy. Ophthalmology 1996;103:561–74.
16. Sonmez K, Drenser KA, Capone A Jr, Trese MT. Vitreous levels of stromal cell-derived factor 1 and vascular endothelial growth factor in patients with retinopathy of prematurity. Ophthalmology 2008;115:1065–70.
17. Krishnan L, Hoying JB, Nguyen H, et al. Interaction of angiogenic microvessels with the extracellular matrix. Am J Physiol Heart Circ Physiol 2007;293:H3650–8.
18. Chung EJ, Kim JH, Ahn HS, Koh HJ. Combination of laser photocoagulation and intravitreal bevacizumab (Avastin) for aggressive zone I retinopathy of prematurity. Graefes Arch Clin Exp Ophthalmol 2007;245:1727–30.
19. Travassos A, Teixeira S, Ferreira P, et al. Intravitreal bevacizumab in aggressive posterior retinopathy of prematurity. Ophthalmic Surg Lasers Imaging 2007;38:233–7.
20. Kusaka S, Shima C, Wada K, et al. Efficacy of intravitreal injection of bevacizumab for severe retinopathy of prematurity: a pilot study. Br J Ophthalmol 2008;92:1450–5.
21. Kong L, Mintz-Hittner HA, Penland RL, et al. Intravitreal bevacizumab as anti-vascular endothelial growth factor therapy for retinopathy of prematurity: a morphologic study [letter]. Arch Ophthalmol 2008;126:1161–3.
22. Geisen P, Peterson LJ, Martiniuk D, et al. Neutralizing antibody to VEGF reduces intravitreous neovascularization and may not interfere with ongoing intraretinal vascularization in a rat model of retinopathy of prematurity. Mol Vis [serial online] 2008;14:345–57. Available at: http://www.molvis.org/molvis/v14/a43/. Accessed April 22, 2009.
23. Honda S, Hirabayashi H, Tsukahara Y, Negi A. Acute contraction of the proliferative membrane after an intravitreal injection of bevacizumab for advanced retinopathy of prematurity. Graefes Arch Clin Exp Ophthalmol 2008;246:1061–3.

Footnotes and Financial Disclosures

Originally received: December 15, 2008.
Final revision: May 7, 2009.
Accepted: May 7, 2009.
Available online: October 8, 2009. Manuscript no. 2008-1501.

The Department of Ophthalmology, National Center for Child Health and Development, Tokyo, Japan.

Financial Disclosure(s):
The authors have no proprietary or commercial interest in any of the materials discussed in this article.

Supported by Grants of Research for Disorders of Sensory Organs from the Ministry of Health Welfare and Labor, Japan.

Correspondence:
Noriyuki Azuma, MD, PhD, Department of Ophthalmology, National Center for Child Health and Development, 2-10-1 Ohkura, Setagaya-ku, Tokyo, 157-8535, Japan. E-mail: azuma-n@ncchd.go.jp.

EDITOR'S CHOICE

Evaluation of filtering bleb function by thermography

S Kawasaki,[1] S Mizoue,[1] M Yamaguchi,[1] A Shiraishi,[1] X Zheng,[1] Y Hayashi,[2] Y Ohashi[1]

[1] Department of Ophthalmology, Medicine of Sensory Function, Ehime University Graduate School of Medicine, Toon-City, Ehime, Japan; [2] Division of Ophthalmology, Minami-Matsuyama Hospital, Matsuyama-City, Ehime, Japan

Correspondence to: Dr S Kawasaki, Department of Ophthalmology, Ehime University School of Medicine, Shitsukawa, Toon-City, Ehime 791-0295, Japan; skawasak@m.ehime-u.ac.jp

Accepted 13 April 2009
Published Online First 10 June 2009

ABSTRACT

Aim: To determine whether thermography can be used to evaluate bleb function.

Methods: The surface temperatures of filtering blebs from 39 eyes of 33 post-trabeculectomy patients were measured using thermography. We introduced a new parameter: the temperature decrease in the filtering bleb (TDB) where TDB = (mean temperature of the temporal and nasal bulbar conjunctiva)−(temperature of the filtering bleb). The eyes were classified into good and poor intraocular pressure (IOP) control groups according to the patients' postoperative IOP. The morphological appearance of the filtering blebs were classified by slit-lamp images according to the Indiana Bleb Appearance Grading Scale. The differences in TDB were analysed statistically.

Results: Mean overall scores were as follows. The TDB were 0.54 (SD 0.20) °C and 0.21 (SD 0.18) °C for the good and poor IOP control groups, respectively. The difference between the TDB of the two IOP control groups was significant ($p<0.0001$), but there was no significant relationship between morphological classification and TDB.

Conclusions: Thermographic measurements suggest that functional blebs have lower temperatures than non-functional blebs, and their morphological appearances are not affected by their temperature. Thermography may be useful for the evaluation of bleb function.

Trabeculectomy is widely performed as a reliable surgical procedure for reducing intraocular pressure (IOP). In postoperative management, slit-lamp biomicroscopy is routinely used to check bleb function. Generally, filtering blebs are classified into three categories: cystic, diffuse and flat blebs.[1 2] A more precise classification system has been introduced recently.[3] The clinical features of well or poorly functioning blebs are well described.[4–6] However, evaluating bleb function by slit-lamp is not always accurate nor easy. To overcome this problem, the internal structure of filtering blebs has been examined by ultrasound biomicroscopy (UBM),[7 8] optical coherence tomography (OCT)[9–11] and in vivo confocal microscopy (Rostock cornea module).[12 13] In spite of such advanced morphological methods, there are still limitations in accuracy and reliability.

Essentially, in a well functioning bleb, aqueous humour flows out of the scleral flap to perfuse the subconjunctival space. We hypothesised that differences in aqueous humour dynamics in filtering blebs might be reflected as differences in surface temperature. Therefore, we tried to measure the temperature of filtering blebs by thermography. Thermography is a non-invasive technique used to measure the surface temperature of an object by detecting the intensity of infrared light that is emitted from the object. It was introduced into the medical field in 1957 by Barnes[14] and has been used in ophthalmology since the mid 1960s,[15] particularly for the diagnosis of dry eye syndrome and other ocular surface disorders.[16–23] However, the temperature of a filtering bleb has never been measured before. In this study, we examined the relationship between bleb function and the temperature of the filtering bleb.

MATERIALS AND METHODS

Study protocol

Thirty-five consecutive patients (41 eyes of 20 men and 15 women) were studied between September 2005 and September 2006. Two patients were excluded from the study because full exposure of the filtering bleb was difficult due to extremely narrow lid fissures and conjunctival scarring, respectively. Therefore, 39 eyes were analysed over 6 months after the last trabeculectomy.

Surgeries were performed in the Ophthalmology Division of Minami Matsuyama Hospital between November 2000 and February 2006. In all cases, a surgical sponge soaked with 0.04% mitomycin C was applied around the site of the scleral flap for 3 min, followed by rinsing with 200 ml of balanced salt solution (Alcon, Fort Worth, Texas, USA).

The type of glaucoma, age, preoperative IOP, postoperative IOP, duration from surgery to thermography, location of the conjunctival flap, and morphological appearance of the filtering bleb were recorded for each patient.

Measurement of ocular surface temperature by thermography

A non-contact thermographic device (TH1106; NEC San-ei Instruments, Tokyo, Japan) was used. This instrument can detect temperatures ranging from −10 °C to 70 °C, with a minimum temperature resolution of 0.025 °C. One second was required to perform each measurement. The temperature data were transformed into a colour-coded image that was displayed in real time on a monitor with a resolution of 256×207 pixels. Its focal range was set from 20 cm to infinity. Using the highest magnification, the ocular surface was measured in one frame, 30.0 mm × 28.4 mm, so that 1 mm^2 was equal to 8×8 pixels when the instrument was positioned 20 cm from the ocular surface. The thermographic device was calibrated using a black body radiator on a regular maintenance schedule.

Each subject was examined in a room at 26.0 (SD 1.5) °C and 40.0 (SD 5.0)% humidity, with standard indoor levels of illumination and no air drafts. We measured the ocular surface temperature after the subject had rested for 15 min in a natural state, according to Kabayama's technique.[16] The thermographic device was set up 20 cm in front of the eye,

and the head was held steady by a head-holder frame. First, the subject was instructed to open his eyes naturally and look straight ahead, and after a blink, a measurement was made. Then, the examiner raised the upper eyelid and instructed the subject to look downward to expose the bleb, and another measurement was made within 1 s. The temperature was measured within 1 s of opening the eye, because ocular surface temperature is known to change during eye opening.[23] Thus the measurement taken at the time point immediately after eyelid opening was thought to reflect most accurately the surface temperature of bleb when it was covered by the eyelid. All thermographic measurements were performed in a special examination room used only for thermography by one examiner who was not given any information about the subjects' IOP control.

To establish the location of the bleb in reference to the cornea and conjunctiva, slit-lamp digital photographs were taken at the same time and the same magnification as the thermograms. Each region of interest, corresponding to the centre of the cornea, the temporal and nasal bulbar conjunctiva, and the filtering bleb, was electronically outlined with a box measuring 16×16 pixels. The computer determined the mean value for the pixels. The temperatures of the temporal and nasal bulbar conjunctiva were determined at the midpoint between the corneal limbus and either the medial or lateral canthus, and the temperature of the filtering bleb was determined at the centre of the scleral flap.

Comparing temperatures as absolute values may not be appropriate, because body temperature varies among individuals. To resolve this problem, we introduced a new parameter:

Table 1 Detailed patient information

Case	IOP control*	Type of glaucoma	Sex	Age (years)	Preop IOP (mmHg)	Postop IOP (mmHg)	Duration from surgery to thermography (months)	Base of the conjunctival flap	IBAGS grade				TDB (°C)
									H	E	V	S	
1	Good	POAG	F	83	37	14	12	Limbal	2	1	1	0	0.55
2	Good	POAG	F	83	30	15	6	Limbal	2	2	1	1	0.30
3	Good	POAG	F	79	17	11	12	Fornix	1	1	1	0	0.55
4	Good	POAG	F	77	24	13	16	Fornix	1	2	3	0	0.35
5	Good	POAG	F	74	17	13	49	Limbal	2	3	1	0	0.45
6	Good	POAG	F	74	35	12	14	Fornix	2	2	2	0	0.45
7	Good	POAG	F	74	24	9	14	Fornix	2	2	2	0	0.25
8	Good	POAG	F	67	33	11	12	Fornix	2	2	0	1	0.70
9	Good	POAG	M	83	20	13	20	Fornix	2	2	0	0	0.60
10	Good	POAG	M	62	31	13	26	Limbal	3	3	1	0	0.45
11	Good	POAG	M	55	16	13	7	Limbal	2	2	1	0	0.70
12	Good	POAG	M	55	16	14	6	Limbal	2	1	1	1	0.40
13	Good	PEG	F	74	18	13	6	Limbal	0	0	2	0	0.85
14	Good	PEG	F	74	18	13	6	Limbal	0	0	3	0	0.95
15	Good	PEG	F	70	24	10	13	Limbal	2	2	3	0	0.20
16	Good	PEG	M	85	20	7	37	Limbal	1	1	2	0	0.45
17	Good	PEG	M	84	25	12	6	Limbal	0	0	3	0	0.40
18	Good	PEG	M	70	35	8	54	Limbal	1	3	0	0	0.45
19	Good	PEG	M	67	28	13	6	Limbal	0	0	3	0	0.95
20	Good	SG-n	F	72	38	8	43	Fornix	2	2	1	0	0.70
21	Good	SG-n	F	66	47	10	14	Fornix	3	2	1	0	0.55
22	Good	SG-u	F	65	24	16	29	Limbal	3	2	1	0	0.70
23	Good	SG-n	M	70	28	16	6	Limbal	3	3	0	1	0.50
24	Poor	POAG	M	82	19	16†	28	Fornix	1	2	3	0	0.25
25	Poor	POAG	M	76	28	14†	12	Limbal	1	2	0	1	0.30
26	Poor	POAG	M	76	18	17‡	40	Limbal	1	1	0	0	0.55
27	Poor	POAG	M	74	18	16‡	43	Limbal	1	1	0	0	0.45
28	Poor	POAG	M	69	28	16†	24	Limbal	0	0	3	0	0.20
29	Poor	POAG	M	48	35	14†	55	Limbal	1	2	2	0	0.05
30	Poor	PEG	M	81	30	15‡	33	Fornix	0	0	2	0	−0.05
31	Poor	PACG	F	69	22	17‡	27	Fornix	0	0	2	0	0.05
32	Poor	POAG	F	77	22	21‡	60	Limbal	1	0	3	0	0.15
33	Poor	POAG	M	72	25	23‡	12	Limbal	1	1	2	0	0.10
34	Poor	POAG	M	70	42	23‡	11	Fornix	1	1	3	0	0.00
35	Poor	POAG	M	66	19	24‡	43	Limbal	2	3	0	0	0.15
36	Poor	PEG	M	79	28	23†	6	Limbal	3	2	3	0	0.40
37	Poor	PEG	M	75	26	21†	12	Fornix	1	1	1	1	0.05
38	Poor	SG-i	F	48	46	24‡	19	Limbal	3	3	1	0	0.20
39	Poor	SG-n	F	40	42	26‡	6	Limbal	3	3	1	0	0.50

E, extent; H, height; IBAGS, Indiana Bleb Appearance Grading Scale; PACG, primary angle-closure glaucoma; PEG, pseudoexfoliation glaucoma; POAG, primary open-angle glaucoma; S, Seidel test; SG, secondary glaucoma caused by neovascularisation of the angle (-n), uveitis (-u), or the iridocorneal endothelial syndrome (-i); TDB, temperature decrease in the filtering bleb: V, vascularity.

*Good: IOP ≤21 mmHg without antiglaucoma medications; poor: filtering blebs with antiglaucoma medications for elevated IOP.

†With two topical medications; ‡with three topical medications.

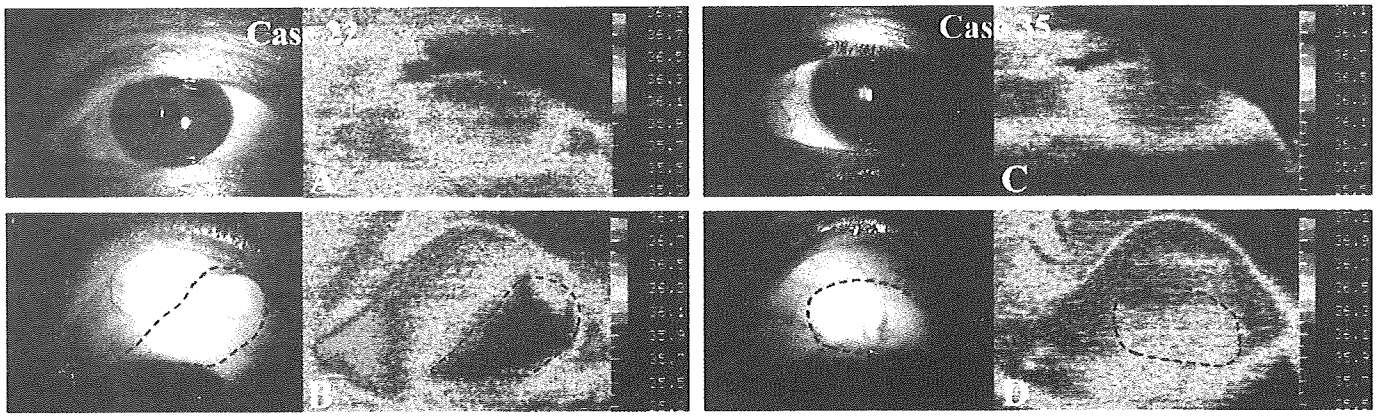

Figure 1 Representative slit-lamp photographs and thermograms from the good and poor intraocular pressure control group are shown. Dotted lines are drawn along the edge of the filtering bleb. Case 22 (A, B) belongs to the good IOP control group and case 35 (C, D) belongs to the poor IOP control group. Each thermogram is divided into eight different colours in 0.2°C steps from dark blue to pink. In the forward gaze (A, C), the cornea is displayed as blue or green and the temporal and nasal bulbar conjunctiva as red or pink. In the downward gaze, the filtering bleb of the good IOP control group (case 22; (B)) is shown as green or blue, meaning that its temperature is clearly lower than that of the surrounding bulbar conjunctiva. Meanwhile, the filtering bleb of the poor IOP control group (case 35; (D)) is represented as yellow or pink, meaning that its temperature is almost same as that of the surrounding bulbar conjunctiva.

the temperature decrease in the filtering bleb (TDB). The temperature of the upper conjunctiva was assumed to be the original temperature of the filtering bleb. Therefore, the mean temperature of the temporal and nasal bulbar conjunctiva was substituted for the temperature of the upper conjunctiva. TDB is described by the equation TDB = (mean temperature of the temporal and nasal bulbar conjunctiva)–(temperature of the filtering bleb).

Classification of subjects according to IOP control

Filtering blebs were classified by IOP control according to criteria from previous studies.[1 2] Functioning blebs, the good IOP control group, were defined as those with an IOP <21 mmHg without antiglaucoma medications, and failed blebs, the poor IOP control group, were defined as those who had received more than two eye drops of antiglaucoma medications for elevated IOP ⩾21 mmHg in the past. The differences between the two groups were examined.

Morphological assessments

It is clinically important to examine whether TDB is affected by the morphological appearance of the filtering bleb. Filtering blebs were classified by slit-lamp examination according to the Indiana Bleb Appearance Grading Scale (IBAGS)[3]; blebs were graded for height (H0–3), extent (E0–3), vascularity (V0–4), and leakage with the Seidel test (S0–2) in a masked manner. We examined the relationship between the morphological appearance and temperature of the filtering blebs.

Table 2 Mean temperatures and statistical analyses of the good and poor intraocular pressure control groups

IOP control group	Cornea	Temporal conjunctiva	Nasal conjunctiva	Filtering bleb	TDB
Good	35.45 (0.53)	35.87 (0.48)	36.01 (0.48)	35.40 (0.50)	0.54 (0.20)
Poor	35.53 (0.50)	35.92 (0.43)	36.05 (0.42)	35.78 (0.43)	0.21 (0.18)
p Value	0.6063	0.6991	0.8523	0.0307*	<0.0001*

IOP, intraocular pressure; TDB, temperature decrease in the filtering bleb.
Values are mean (SD).
*Mann–Whitney U test.

Statistical analyses

The χ^2 test, Fisher's exact test, Mann–Whitney U test or ANOVA were used to determine the statistical significance of any differences. The level of significance was set at $p<0.05$. Pearson's correlation coefficient was used for examining correlation, and intraclass correlation coefficients were used for examining the reproducibility of our thermographic measurements.

RESULTS

The details of the subjects are summarised in table 1. The mean age of the subjects at the time of thermography was 70.9 (SD 10.4) (range 40–85) years. There were 23 filtering blebs in the good IOP control group and 16 filtering blebs in the poor IOP control group. No significant differences between the two groups were found in the type of glaucoma ($p = 0.5193$, χ^2 test), age ($p = 0.6675$, Mann–Whitney U test), preoperative IOP ($p = 0.4656$, Mann–Whitney U test), time from surgery to thermography ($p = 0.1270$, Mann–Whitney U test) or site of the base of the conjunctival flap ($p>0.9999$, Fisher's exact test).

Reproducibility

The reproducibility of our thermographic measurements was examined. Thermography was performed three times at intervals of more than 1 min in 11 eyes in forward gaze and 22 eyes in downward gaze that were selected randomly from the subjects. The intraclass correlation coefficients for the temperature at the centre of the cornea, the temporal bulbar conjunctiva, the nasal bulbar conjunctiva and the filtering bleb were 0.9748, 0.9811, 0.9768 and 0.9680, respectively.

Correlation between IOP reduction and TDB

In this study, there were 13 well-functioning blebs that received full antiglaucoma medications (three or more eyedrops with oral acetazolamide therapy) before trabeculectomy (cases 1, 2, 4, 6–8, 10, 15, 17, 18, 20, 21 and 23). We examined the correlation between IOP reduction and TDB in these 13 cases. The mean IOP reduction was 20.9 (SD 7.4) mmHg and the mean TDB was 0.43 (SD 0.15) C. The two factors were correlated (Pearson's correlation coefficient: 0.6822, $p = 0.010196$).

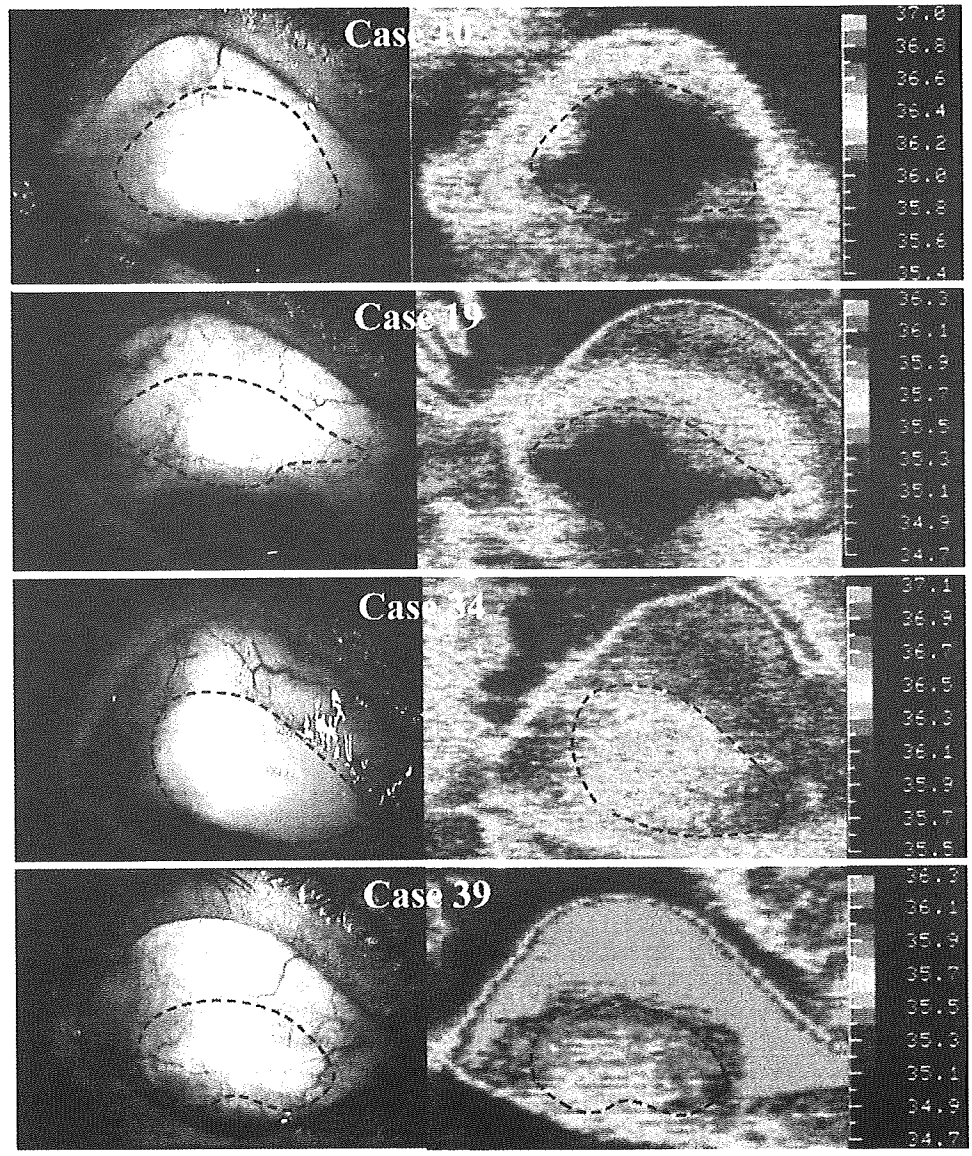

Figure 2 Representative thermograms of both cystic and flat blebs in the good and poor intraocular pressure control groups are shown. Dotted lines are drawn along the edge of the filtering bleb. Cases 10 and 19 belong to the good IOP control group and cases 34 and 39 belong to the poor IOP control group. In the good IOP control group, the temperature of the filtering bleb is clearly lower than that of the surrounding bulbar conjunctiva, even if no cystic bleb is recognised in the slit-lamp examination. In the poor IOP control group, the temperature of the filtering bleb is almost the same as that of the surrounding bulbar conjunctiva, even if a filtering bleb with a cystic appearance is present.

Comparison of ocular surface temperature

Ocular surface temperatures and statistical analyses of the good and poor IOP control groups are listed in table 2. There were significant differences between both the temperature of the filtering bleb and the TDB of the two groups. Figure 1 shows typical thermograms of the good (case 22 (fig 1A, B) and poor (case 35 (fig 1C, D)) IOP control groups. The temperature of the filtering bleb was clearly lower than that of the surrounding bulbar conjunctiva in the good IOP control group, while the temperature of the filtering bleb was almost the same as that of the surrounding bulbar conjunctiva in the poor control group.

Effects of morphological appearance

We examined the relationship of TDB to the morphological appearance of the filtering blebs classified based on the IBAGS[5] (table 3). Statistical analyses showed no significant relationship between the TDB and any of the morphological factors. Figure 2 displays thermograms of cystic and flat blebs from each of the two groups. In the good IOP control group (cases 10 and 19), the temperature of the filtering bleb was lower than that of the surrounding bulbar conjunctiva, irrespective of its morphology. In the poor IOP control group (cases 39 and 34), the temperature of the filtering bleb was almost the same as that of the surrounding bulbar conjunctiva.

In addition, we examined the blebs to determine whether there were differences between the morphological appearances of the good and poor IOP control groups. Statistical analyses showed that the differences between the two groups were not significant (height (H) $p = 0.1580$; extent (E) $p = 0.3872$; vasularity (V) $p = 0.6043$; Seidel test (S): $p = 0.7546$; Mann–Whitney U test).

DISCUSSION

In the present study, we showed that the mean surface temperature of the filtering blebs in the good IOP control group was lower than that of the poor IOP control group. Furthermore, we introduced a thermographic index, TDB, to correct for body temperature, which varies among individuals. The TDB of the good IOP control group was significantly lower than that of the poor IOP control group. It could be argued that the morphological appearance, especially the vascularity, of the filtering bleb may affect its temperature. In this study, a thermographic measurement of each filtering bleb was made within 1 s after exposing the bleb, and as shown in table 3, there

Table 3 Relationship of TDB to the morphological appearance of the filtering blebs determined based on the IBAGS

IBAGS grade	n	TDB (°C)	p Value
Height (H)			
0	7	0.479 (0.434)	
1	13	0.285 (0.198)	0.2231*
2	12	0.454 (0.199)	
3	7	0.471 (0.152)	
Extent (E)			
0	8	0.438 (0.418)	
1	9	0.344 (0.228)	0.8453*
2	15	0.433 (0.214)	
3	7	0.386 (0.146)	
Vascularity (V)			
0	8	0.462 (0.173)	
1	13	0.469 (0.196)	0.3183*
2	8	0.269 (0.300)	
3	10	0.385 (0.321)	
Seidel test (S)			
0	33	0.411 (0.263)	0.7546†
1	6	0.375 (0.219)	

IBAGS, Indiana Bleb Appearance Grading Scale; TDB, temperature decrease in the filtering bleb.
Values are mean (SD).
*ANOVA; †Mann–Whitney U test.

was no significant correlation between the TDB and the morphological appearance of the filtering blebs as determined by the IBAGS.[3] Thus, the surface temperature of the filtering bleb was correlated with postoperative IOP control, regardless of whether the morphological appearance appeared flat or vascularised. These results imply that thermography may be useful to assess bleb function.

Some morphological approaches have been developed recently to assess bleb function. UBM has been widely used because it provides useful information through images of the scleral flap and its surrounding structure. However, assessments of bleb function using UBM are sometimes unreliable.[10] In one study,[7] the IOP was assessed as poor in six of 89 eyes with Type L blebs where the actual IOP was generally good. In another study,[2] phacoemulsification significantly increased the IOP in eyes with filtering blebs, but the intrableb features did not change in the UBM image. Anterior segment OCT has been introduced to assess bleb function as a non-invasive examination. Generally, OCT shows that a functional bleb has a large hyporeflective space with a collection of fluid. Savini *et al* reported that hyporeflective fluid-filled spaces were not clearly visualised in two of 21 eyes with the good IOP control.[9] Leung *et al* reported that subconjunctival fluid spaces could not be detected in two flattened blebs with good IOP control.[10] Singh *et al* found that the majority of successful blebs demonstrated thickening of the bleb wall, but thickening was also found in six of 21 failed blebs.[11] Thus, there are some limitations in the accuracy of these methods for assessing bleb function.

In a well functioning bleb, the aqueous humour flows continuously out of the scleral flap to perfuse the subconjunctival space around the filtering bleb. In a poorly functioning bleb, on the other hand, the amount of aqueous humour flowing into the filtering bleb is small, and therefore the aqueous humour turnover in the subconjunctival space is reduced. In a report by Heys *et al*, when the temperature of the ciliary body and the iris was specified to be 37.0°C, the temperature of the aqueous humour near the cornea was calculated to be 34.4°C.[4] Since aqueous humour cooler than the surrounding tissue is constantly flowing through a well-functioning bleb, this may cause the temperature of the cornea and filtering bleb to decrease to a level lower than that of the surrounding conjunctiva. On the other hand, a poorly functioning bleb is warmed by the eyelid and the conjunctiva, and therefore its temperature would be expected to remain the same as the surrounding tissue. Thermography may capture this phenomenon. Even if no cystic bleb is recognised in a slit-lamp examination, thermography can detect an area at the site of the scleral flap that is cooler than the surrounding bulbar conjunctiva, indicating that fresh aqueous humour may be flowing in the subconjunctival space around a filtering bleb (see case 19 in fig 2). Furthermore, even if a filtering bleb with a cystic appearance is present, thermography can show that the bleb is not functional; if an area cooler than the surrounding bulbar conjunctiva is not detected at the site of the scleral flap, this indicates that aqueous humour may not be flowing efficiently (see case 35 in fig 1 and case 39 in fig 2).

The TDB of each subject is shown in table 1. If the threshold level of the TDB for a well functioning bleb is defined to be ≥0.40 C, there are 19 filtering blebs (82.6%) in the good IOP control group and four filtering blebs (25.0%) in the poor IOP control group. These results are significantly correlated with bleb function ($p = 0.0007$; Fisher' exact test). We examined the four exceptional filtering blebs in the poor IOP control group by UBM. The results of UBM suggested that two filtering blebs (case 26 and 39) were poorly functional (type E: encapsulated bleb); however the other filtering blebs (case 27 and 36) were fairly functional (type H: high-reflective bleb) according to Yamamoto's classification.[7] Unfortunately, we are unable to explain why the IOP was elevated in the latter two cases, suggesting that similar to OCT and UBM, our thermographic method also has limitations. Thus, the efficiency of evaluating bleb function can be improved by using a combination of multiple examinations including OCT and UBM. In addition, improved software or more accurate instruments may be helpful to carry out more precise examinations. In this regard, we are developing an instrument that is specifically suitable for ocular surface thermography.

In conclusion, thermography sheds new insight on the evaluation of bleb function and may become another useful method for evaluating bleb function.

Competing interests: None declared.

Ethics approval: The procedures used in this study conformed to the guidelines adopted by the Declaration of Helsinki. The Institutional Review Board of the Ehime University Graduate School of Medicine and Minami Matsuyama Hospital approved the experimental protocol.

Patient consent: Obtained.

Provenance and peer review: Not commissioned; externally peer reviewed.

REFERENCES

1. **Vesti E.** Filtering blebs: follow up of trabeculectomy. *Ophthalmic Surg* 1993;**24**:249–55.
2. **Picht G,** Grehn F. Classification of filtering blebs in trabeculectomy: biomicroscopy and functionality. *Curr Opin Ophthalmol* 1998;**9**:2–8.
3. **Cantor LB,** Mantravadi A, WuDunn D, *et al*. Morphologic classification of filtering blebs after glaucoma filtration surgery: the Indiana Bleb Appearance Grading Scale. *J Glaucoma* 2003;**12**:266–71.
4. **Hu CY,** Matsuo H, Tomita G, *et al*. Clinical characteristics and leakage of functioning blebs after trabeculectomy with mitomycin-C in primary glaucoma patients. *Ophthalmology* 2003;**110**:345–52.
5. **Migdal C,** Hitchings R. The developing bleb: effect of topical antiprostaglandins on the outcome of glaucoma fistulising surgery. *Br J Ophthalmol* 1983;**67**:655–60.
6. **Richter CU,** Shingleton BJ, Bellows AR, *et al*. The development of encapsulated filtering blebs. *Ophthalmology* 1988;**95**:1163–8.
7. **Yamamoto T,** Sakuma T, Kitazawa Y. An ultrasound biomicroscopic study of filtering blebs after mitomycin C trabeculectomy. *Ophthalmology* 1995;**102**:1770–6

8. **Wang X,** Zhang H, Li S, *et al*. The effects of phacoemulsification on intraocular pressure and ultrasound biomicroscopic image of filtering bleb in eyes with cataract and functioning filtering blebs. *Eye* 2009;**23**:112–16.
9. **Savini G,** Zanini M, Barboni P. Filtering blebs imaging by optical coherence tomography. *Clin Experiment Ophthalmol* 2005;**33**:483–9.
10. **Leung CK,** Yick DW, Kwong YY, *et al*. Analysis of bleb morphology after trabeculectomy with the Visante anterior segment optical coherence tomography. *Br J Ophthalmol* 2007;**91**:340–4.
11. **Singh M,** Chew PT, Friedman DS, *et al*. Imaging of trabeculectomy blebs using anterior segment optical coherence tomography. *Ophthalmology* 2007;**114**:47–53.
12. **Messmer EM,** Zapp DM, Mackert MJ, *et al*. In vivo confocal microscopy of filtering blebs after trabeculectomy. *Arch Ophthalmol* 2006;**124**:1095–103.
13. **Labbe A,** Dupas B, Hamard P, *et al*. In vivo confocal microscopy study of blebs after filtering surgery. *Ophthalmology* 2005;**112**:1979–86.
14. **Barnes RB.** Thermography of the human body. *Science* 1963;**140**:870–7.
15. **Mapstone R.** Ocular thermography. *Br J Ophthalmol* 1970;**54**:751–4.
16. **Kabayama T,** Suzuki H, Horiuchi T, *et al*. Ganka Thermography No Kenkyu [Studies on thermography—its clinical application for ophthalmology]. *Nippon Ganka Gakkai Zasshi* 1979;**83**:326–35.
17. **Efron N,** Young G, Brennan NA. Ocular surface temperature. *Curr Eye Res* 1989;**8**:901–6.
18. **Morgan PB,** Soh MP, Efron N, *et al*. Potential applications of ocular thermography. *Optom Vis Sci* 1993;**70**:568–76.
19. **Morgan PB,** Tullo AB, Efron N. Infrared thermography of the tear film in dry eye. *Eye* 1995;**9**:615–8.
20. **Mori A,** Oguchi Y, Okusawa Y, *et al*. Use of high-speed, high-resolution thermography to evaluate the tear film layer. *Am J Ophthalmol* 1997;**124**:729–35.
21. **Craig JP,** Singh I, Tomlinson A, *et al*. The role of tear physiology in ocular surface temperature. *Eye* 2000;**14**:635–41.
22. **Purslow C,** Wolffsohn JS. Ocular surface temperature: a review. *Eye Contact Lens* 2005;**31**:117–23.
23. **Purslow C,** Wolffsohn J. The relation between physical properties of the anterior eye and ocular surface temperature. *Optom Vis Sci* 2007;**84**:197–201.
24. **Heys JJ,** Barocas VH. A boussinesq model of natural convection in the human eye and the formation of Krukenberg's spindle. *Ann Biomed Eng* 2002;**30**:392–401.

Genetic Dissociation of Dacryoadenitis and Sialadenitis in a Sjögren's Syndrome Mouse Model with Common and Different Susceptibility Gene Loci

Tomoyuki Kamao,[1,2] *Tatsuhiko Miyazaki,*[1] *Yoshiko Soga,*[1] *Hiroaki Komori,*[1] *Miho Terada,*[1] *Yuichi Ohashi,*[2] *and Masato Nose*[1]

Purpose. Sjögren's syndrome (SS) is a systemic autoimmune disease in which the main lesions are dacryoadenitis and sialadenitis. It is unclear whether these lesions develop in a common genetic background. A quantitative trait locus (QTL) analysis was performed in the SS mouse model, MRL/MpJ-*lpr/lpr* (MRL/lpr), to identify the susceptibility loci to dacryoadenitis and sialadenitis and the association with both loci.

Methods. MRL/lpr, C3H/HeJ-*lpr/lpr* (C3H/lpr), (MRL/lpr × C3H/lpr) F1, and (MRL/lpr × C3H/lpr) F2 intercross mice were prepared, and the severity of dacryoadenitis and sialadenitis in individuals was quantified by histopathologic grading. In genomic DNA samples from the F2 mice, the polymorphic microsatellite markers highly associated with each lesion were determined as susceptibility loci.

Results. QTLs with significant linkage for dacryoadenitis were mapped on chromosome 1 (the position of maximum logarithm of odds [LOD] score; 64.1 cM), designated *Adacm1*; chromosome 2 (88.4 cM), *Adacm2*; and chromosome 5 (63.9 cM), *Adacm3*. Those for sialadenitis were mapped on chromosome 1 (69.0 cM), *Asm3*, and chromosome 2 (65.3 cM and 82.1 cM), *Asm4* and *Asm5*. *Adacm1/Asm3* and *Adacm2/Asm5* seemed to be a common chromosomal region, respectively. MRL-homozygous at *Adacm1* and *Adacm2* and at *Asm3* and *Asm5* manifested an additive effect on the development of dacryoadenitis and sialadenitis, respectively, whereas *Adacm3* did not.

Conclusions. Dacryoadenitis and sialadenitis in MRL/lpr mice are under the control of common and different susceptibility loci, with an allelic combination that leads to regular variations in pathologic phenotypes. (*Invest Ophthalmol Vis Sci.* 2009; 50:3257–3265) DOI:10.1167/iovs.08-3132

Sjögren's syndrome (SS) is a systemic autoimmune disease. However, the main lesions in SS are in the lacrimal glands and salivary glands, associated with autoimmune mechanisms. These lesions are commonly characterized by the destruction of the ductules at their beginning, by the accumulation of mononuclear cells followed by destruction of the acinar glands.[1] However, it is unclear whether these lesions develop in a common genetic background.

An investigation of the clinical symptoms in patients with SS showed that the incidence of dry eye is 67.5% and that of dry mouth is 93.5%,[2] when based on the European Community criteria.[3] Other studies showed that the frequency of both symptoms in SS is 82.5%,[4] according to the revised European classification criteria.[5,6] These results suggest that almost 20% to 30% of patients with SS do not have either dry eye or dry mouth. Although the laboratory tests in patients with SS revealed that 80.7% of the patients with SS are positive for the ocular component and 94.7% of those are positive for the oral component.[1] This result means that almost 20% of patients with SS do not have either dysfunction of the lacrimal glands or salivary glands. Histologic examinations of biopsy specimens from lacrimal glands and minor salivary glands in patients with SS showed that 69.2% of patients with SS met the histopathologic criteria of dacryoadenitis and 88.8% of those met that of sialadenitis, based on the revised Japanese criteria.[7] As for this result, the histopathologic manifestations may show the same tendency of the clinical symptoms and laboratory tests. Therefore, the development of dacryoadenitis and sialadenitis in patients with SS may not always be coincidental.

In general, autoimmune diseases show the complex pathologic manifestations involving various lesions such as vasculitis, glomerulonephritis, arthritis, and/or sialadenitis. It remains controversial whether such a complex disease is a manifestation of advanced disease or of multigenic disease with a different gene combination that might be categorized into distinct disease entities. To clarify whether dacryoadenitis and sialadenitis in SS have common genetic mechanisms, we used a SS model, an MRL/Mp-*lpr/lpr* strain of mice.[8] MRL/lpr mice spontaneously develop progressive dacryoadenitis and sialadenitis and other autoimmune diseases such as lupus-like nephritis, arthritis, and vasculitis, in association with immunologic abnormalities.[8–10] Dacryoadenitis and sialadenitis in MRL/lpr mice are histopathologically characterized initially by mononuclear cell infiltration into periductular regions, followed by the progressive destruction of ductules and parenchyma, resembling SS, and thus these mice provide a SS model.[10–12]

The lymphoproliferative gene, *lpr*, is a mutation of the *Fas* gene,[13] which causes an insufficiency of Fas-mediated apoptosis in T and B cells and activated macrophages.[14,15] Therefore, this mutant gene plays an important role in the mechanisms of development of autoimmune diseases in MRL/lpr mice. MRL/lpr mice develop autoimmune diseases, whereas other strains of mice carrying the *lpr* gene, such as C3H/HeJ and C57BL/6J, do not.[16] Moreover, MRL mice have the genes that make them susceptible to each lesion. That is, lupus-like nephritis, arthritis, vasculitis, and sialadenitis in MRL/lpr mice were genetically dissociated in crossing with non-autoimmune-prone *lpr* mice.[17–21]

In the past, many susceptibility loci associated with SS have been demonstrated with various mouse models.[21–24] However, all these studies focused on the salivary glands. There has so far

From the Departments of [1]Pathogenomics and [2]Ophthalmology, Ehime University Graduate School of Medicine, Ehime, Japan.

Supported by Grant-in-Aid for Scientific Research (B) 18390123 of the Ministry of Education, Science and Culture of Japan (MN).

Submitted for publication November 10, 2008; revised December 23, 2008, and January 18, 2009; accepted May 1, 2009.

Disclosure: **T. Kamao**, None; **T. Miyazaki**, None; **Y. Soga**, None; **H. Komori**, None; **M. Terada**, None; **Y. Ohashi**, None; **M. Nose**, None

The publication costs of this article were defrayed in part by page charge payment. This article must therefore be marked "*advertisement*" in accordance with 18 U.S.C. §1734 solely to indicate this fact.

Corresponding author: Masato Nose, Department of Pathogenomics, Ehime University Graduate School of Medicine, 454 Shitsukawa, Toon, Ehime 791-0295, Japan; masanose@m.ehime-u.ac.jp.

been no study in which the susceptibility loci for dacryoadenitis were identified. Of course, the commonality of susceptibility loci of dacryoadenitis and sialadenitis has not yet been determined.

Our study confirmed the difference in the severity of dacryoadenitis and sialadenitis between MRL/lpr and C3H/lpr mice, independently from the MHC, since both strains have an H-2^k haplotype. Therefore, using F2 intercross with MRL/lpr and C3H/lpr mice, we clarified the mode of inheritance of dacryoadenitis and sialadenitis in the MRL, background and the non-MHC gene loci susceptible to them were identified. This is the first report to our knowledge to identify whether autoimmune dacryoadenitis and sialadenitis in MRL mice have common susceptibility loci.

Materials and Methods

Mice

MRL/lpr and C3H/lpr mice were originally purchased from The Jackson Laboratory (Bar Harbor, ME). Both strains were bred and housed under specific pathogen-free conditions in the Animal Research Institute of Tohoku University Graduate School of Medicine, Sendai, and the Department of Biological Resources, the Integrated Center for Science, Ehime University. From these strains, 71 MRL/lpr, 80 C3H/lpr, 40 (MRL/lpr × C3H/lpr) F1 (MCF1) and 527 (MRL/lpr × C3H/lpr) F2 (MCF2) mice were prepared in the same institutes. All procedures involving mice adhered to the ARVO Statement for the Use of Animals in Ophthalmic and Vision Research and the guidelines for laboratory animal experiments.

Histopathologic Evaluation of Dacryoadenitis and Sialadenitis

At 16 to 20 weeks of age, the mice were dissected while under ether anesthesia. The lacrimal glands and submandibular glands were removed, fixed with 10% formalin in 0.01 M phosphate buffer (pH 7.2) and embedded in paraffin. Each section of lacrimal glands and submandibular glands, bilaterally, was stained with hematoxylin-eosin (HE) and histopathologically examined by light microscopy for dacryoadenitis and sialadenitis, respectively, in which 10 or more ductules in each organ were randomly selected for grading the lesion. MCF2 mice developed a variety of phenotypes for dacryoadenitis and sialadenitis. Some of them showed both dacryoadenitis and sialadenitis, and others showed dacryoadenitis or sialadenitis alone (Fig. 1).

The histopathologic examinations for dacryoadenitis and sialadenitis were performed as described elsewhere.[21] The findings were graded on a scale of 0 to 3, where 0 is normal; 1 is mononuclear cell infiltration localized in periductular regions, but no destruction of the parenchyma or ductules; 2 is cell infiltration into duct epithelium, with or without extending to acinar parenchyma; and 3 is grade 2 changes with fibrosis and/or granulation and/or regenerative ductal hyperplasia (Fig. 2). The grading score of each mouse is represented by the index, which was the mean of the individual grading score of 10 or more ductules randomly selected in the histologic section.

Genotyping of MCF2 Mice

Genomic DNA of 527 MCF2 mice was extracted from the tail or liver. The genotyping of MCF2 was determined by simple sequence-length polymorphism analysis with 119 polymorphic microsatellite markers that were purchased from Research Genetics (Huntsville, AL). The map positions of the microsatellite loci were based on Mouse Genome Informatics (MGI, http://www.informatics.jax.org/ provided in the public domain by the Jackson Laboratory).[25] They were an average of 12 cM apart, with a maximum distance between any two markers of 37 cM. Briefly, a total volume of 20 μL of polymerase chain reaction (PCR) mixture (200–300 ng of genomic DNA, 2 μL of 10× PCR buffer [Takara, Tokyo, Japan], 1.6 μL of dNTP mixture [2.5 mM each; Takara], 0.4 units of *Taq* polymerase [Ex *Taq*; Takara], and 0.16 μM of each primer) was prepared for PCR and amplified (GeneAmp PCR System 9600; Perkin Elmer, Wellesley, MA), by using the following thermocycling protocol: 94°C for 2 minutes, followed by 40 cycles of 94°C for 30 seconds, 55 to 60°C for 30 seconds, 72°C for 30 seconds, and 72°C for 5 minutes.

The PCR products were separated by electrophoresis on 2% to 5% agarose gels or standard denaturing 10% polyacrylamide gels. The genotypes of the PCR products from the MCF2 intercross mice were designated MRL/MRL (M) and C3H/C3H (C) homozygotes or MRL/C3H (H) heterozygotes based on size differences.

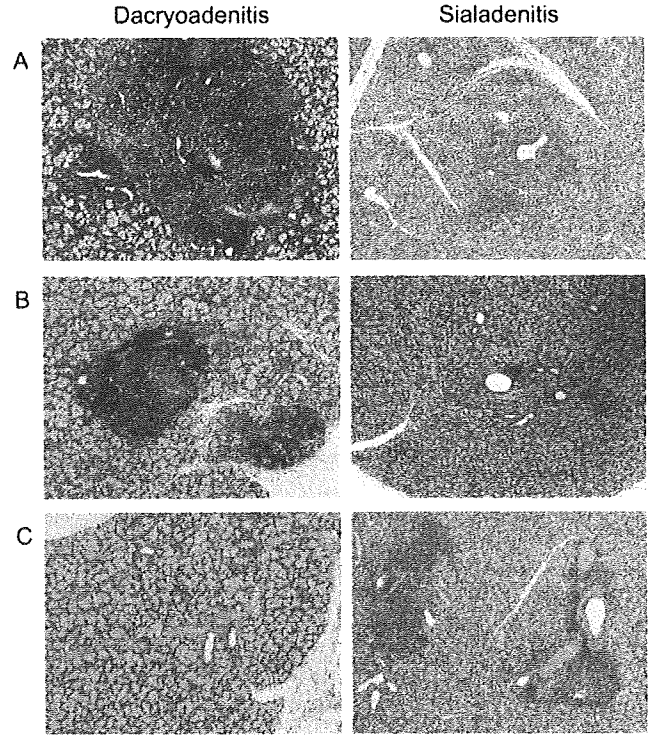

Figure 1. Dissociation of histopathologic phenotypes of dacryoadenitis and sialadenitis in 5-month-old MCF2 intercrossed female mice. (HE stain) (**A**) Dacryoadenitis and sialadenitis, showing marked parenchymal destruction associated with mononuclear cell infiltration into the ductules and extending to the parenchyma. (**B**) Dacryoadenitis without sialadenitis. (**C**) Sialadenitis without dacryoadenitis.

Genome-Wide Screening and QTL Analysis

Initially, the genotyping of each microsatellite marker and phenotyping of each histologic index was performed in the 266 MCF2 mice. Linkage studies on 266 MCF2 mice were performed. Markers with $P \leq 0.01$ were selected (selective genotyping).

Next, linkage studies on another 261 MCF2 mice were performed on the chromosomes bearing the marker showing $P < 0.01$ by using the markers compiled in the first selection. The linkage map for the MCF2 mice was created with Mapmaker3.[26] A linkage analysis was performed on each candidate chromosome with WinQTL Cartographer (ver. 2.5),[27,28] based on each histologic index as the indicators of phenotype. A logarithm of odds (LOD) was calculated using the LR-mapqtl program. Composite interval mapping was performed using model 6 of the ZMapqtl program with options set at 2-dM intervals and a 10-cM window size, considering background loci that included unlinked and linked loci-positioned forward parameters.[28,29] The experiment-wise significance level for each index was determined by analyzing 10,000 random shuffling permutations of the actual data and the results of chromosomes with significant linkages[30] ($\alpha < 0.01$) for either index are shown in the Results section.

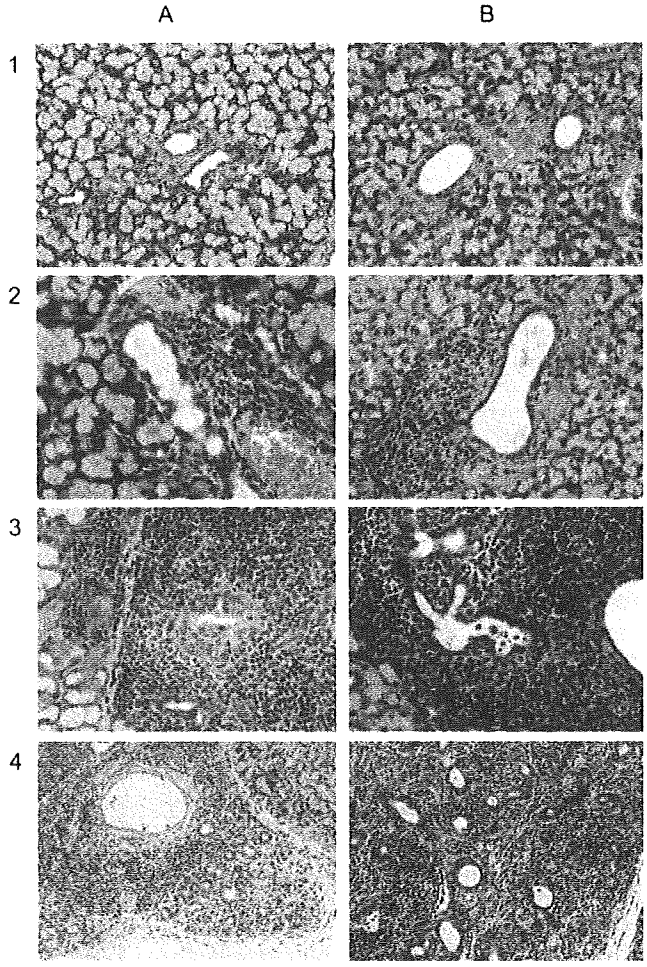

FIGURE 2. Histopathologic grades of dacryoadenitis (**A**) and sialadenitis (**B**) (HE stain). (**1**) Grade 0, no inflammatory cell infiltration, (**2**) grade 1, mononuclear cell infiltration with limited localization in the periductular regions, but no destruction of the parenchyma or ductules; (**3**) grade 2, cell infiltration into the duct epithelium extending to the acinar parenchyma; and (**4**) grade 3, significant parenchymal destruction with regenerative ductal hyperplasia and fibrotic change.

Statistical Analysis

Comparisons of the histologic indexes between parental strains of mice and other generations of mice and interactions among three loci were performed with the Tukey-Kramer test and between females and males in MRL/lpr and MCF2 progeny with the unpaired *t*-test.

RESULTS

Phenotypic Analyses of MRL/lpr, C3H/lpr, MCF1, and MCF2 Mice

The phenotypic analyses for dacryoadenitis and sialadenitis were represented by the index (Fig. 3). The indexes of MRL parents for both lesions were females, (mean score of index ± SD, dacryoadenitis, 1.63 ± 0.57; sialadenitis; 1.15 ± 0.50; Fig. 3B), males (dacryoadenitis, 0.51 ± 0.37; sialadenitis, 0.71 ± 0.29; Fig. 3C) and both of them (dacryoadenitis, 1.28 ± 0.73; sialadenitis, 0.97 ± 0.47; Fig. 3A). Conversely, C3H parents of females (dacryoadenitis, 0.28 ± 0.26; sialadenitis, 0.17 ± 0.24), males (dacryoadenitis, 0.01 ± 0.04; sialadenitis, 0.03 ± 0.07), and both (dacryoadenitis, 0.14 ± 0.23; sialadenitis, 0.10 ± 0.19) hardly developed these lesions.

MCF1 hybrids had a phenotype similar to that of their C3H parents in the females (dacryoadenitis, 0.41 ± 0.25; sialadenitis, 0.20 ± 0.15), the males (dacryoadenitis, 0.05 ± 0.07; sialadenitis, 0.26 ± 0.26), and both (dacryoadenitis, 0.22 ± 0.26; sialadenitis, 0.24 ± 0.23). Scores for both lesions in MRL parents were significantly higher than those in C3H parents and MCF1 hybrids ($P < 0.001$, respectively), which means that both dacryoadenitis and sialadenitis are inherited recessively in mice with an MRL background. Both lesions in females and dacryoadenitis in males showed the same results, and so these were inherited recessively in mice with an MRL background as well. Sialadenitis in males showed an additive manner of inheritance because the MCF1 hybrids had significantly higher indexes than did the C3H parents ($P < 0.001$).

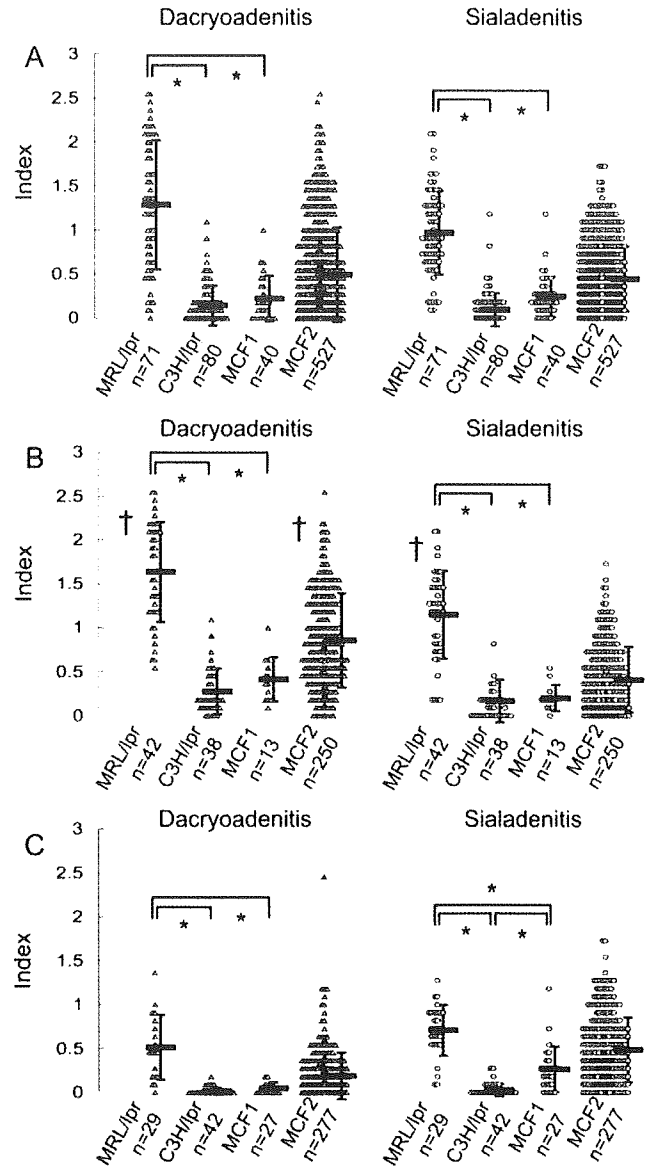

FIGURE 3. A quantitative analysis of dacryoadenitis and sialadenitis indexes (mean and SD) in MRL/lpr, C3H/lpr, their F1 and F2 progenies in both (**A**), females (**B**), and males (**C**). The grade score of each mouse is presented by an index that is the mean of the individual grade of each ductule randomly selected on the histologic section (*circle*). A comparison of the means was performed among the four groups by Tukey-Kramer test, $^*P < 0.001$, and between females and males in MRL/lpr and MCF2 progeny using unpaired *t*-test, $\dagger P < 0.001$.

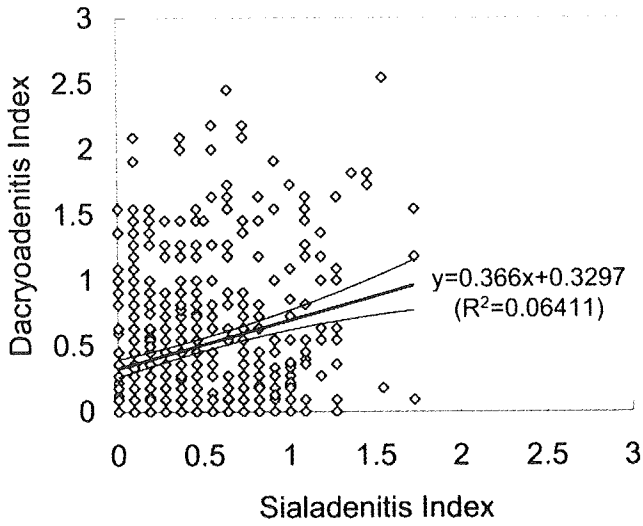

FIGURE 4. Correlation between dacryoadenitis and sialadenitis in MCF2 ($n = 527$). The indexes of each mouse are presented in the x-axis (sialadenitis) and y-axis (dacryoadenitis). Their correlation was estimated by using the Pearson product-moment correlation coefficient. There was only a slight positive correlation between both ($R^2 = 0.06411$; $P < 0.001$). Line of regression (*heavy line*) and confidence interval (*thin line*) are shown on the graph.

MCF2 progeny developed various severities of dacryoadenitis and sialadenitis in the females (dacryoadenitis, 0.85 ± 0.54; sialadenitis, 0.41 ± 0.37), the males (dacryoadenitis, 0.19 ± 0.27; sialadenitis, 0.49 ± 0.37), and both (dacryoadenitis, 0.49 ± 0.53; sialadenitis, 0.45 ± 0.37). In the MCF2 progeny, the same tendency was seen—namely, that the dacryoadenitis and sialadenitis indexes were higher than in C3H parents and MCF1 progeny, but they presented a wide range of the indexes covering those of MRL parents. Dacryoadenitis scores of MRL/lpr and MCF2 progeny and sialadenitis scores of MRL/lpr in females were significantly higher than those in the males ($P < 0.001$, respectively). The penetrance of dacryoadenitis was higher in the females than in the males in the MCF2 intercrossed mice, similar to their MRL parents.

Distribution of Indexes of Both Lesions in MCF2 Progeny

In the next series of experiments, we investigated whether dacryoadenitis and sialadenitis developed associatively in MCF2 progeny (Fig. 4). The individual index of both lesions was discretely distributed. Some of the individuals showed higher indexes in both lesions, some of them were higher in either dacryoadenitis or sialadenitis, and others were lower in both lesions. Only a small positive correlation was observed between dacryoadenitis and sialadenitis ($R^2 = 0.06411$, $P < 0.001$).

Mapping of Dacryoadenitis and Sialadenitis Susceptibility Loci in MCF2 Progeny

A genome-wide scan was performed as described in the Materials and Methods section on the 266 MCF2 progeny with a total of 119 microsatellite markers, and an association study was conducted. In chromosomes 1, 2, 5, and 9, there was at least one microsatellite marker on one chromosome that fulfilled the standard of $P < 0.01$.

A QTL analysis of these candidate chromosomes using all 527 MCF2 progeny demonstrated that chromosomes 1 and 2 had the highest LOD scores with significant linkage for both dacryoadenitis and sialadenitis. The highest peak on chromosome 5 was limited to one with significant linkage only for dacryoadenitis (Fig. 5). The highest LOD scores for chromosome 1 were 4.0 (map position 64.1 cM) for dacryoadenitis and 16.8 (69.0 cM) for sialadenitis. These positions were susceptibility loci in the region of an MRL allele and were designated *Adacm1* and *Asm3*. On chromosome 2, the highest LOD score for dacryoadenitis was 3.7 (88.4 cM) and sialadenitis was 5.6 (65.3 cM). These positions were also susceptibility loci in the region of an MRL allele, designated *Adacm2* and *Asm4*, respectively. A LOD score of the second highest peak on chromosome 2 was 5.4 (82.1 cM) for sialadenitis, close to *Asm4*, also a susceptibility locus in the region of an MRL allele, designated *Asm5*. On chromosome 5, the highest LOD score for dacryoadenitis was 3.1 (63.9 cM), also a susceptibility locus in the region of an MRL allele, designated *Adacm3*. Regarding chromosome 9, there were no loci with a significant linkage, but only suggestive (LOD score; 2.6) for dacryoadenitis in the females.

The best model to fit the inheritance of these susceptibility loci was determined with the WinQTL Cartographer program. The results are summarized in Table 1. *Adacm1* and *Asm3*, *-4*, and *-5* corresponded to an additive manner of inheritance, whereas *Adacm1* and *-2* corresponded to recessive. These adjustments were confirmed by nonparametric tests. None of these loci was protective. As shown in Figure 5, *Adacm1* was located very close to *Asm3* and *Adacm2* was to *Asm5*. Each of the two loci seemed to be located in the common chromosomal region, whereas *Adacm3* and *Asm4* were independent from any other loci.

Interaction Analysis of the Loci

The interactions of the two loci for dacryoadenitis and sialadenitis were investigated to clarify the relationships among the multiple loci which were identified (Table 2). Since *Adacm2* on chromosome 2 and *Adacm3* on chromosome 5 were recessive as shown in Table 1, mice with H and C genotypes at the *D2Mit285* and *D5Mit136* markers, respectively, were grouped. The other four loci, that is to say *Asm3*, *-4*, and *-5* and *Adacm1*, showed an additive mode in inheritance (Table 1). It disclosed a complex pattern of interaction, so a comparison of M to C was examined at the related markers, respectively.

First, each of the two loci, which seemed to be located in a common chromosomal region (*Adacm1* and *-2*, or *Asm3* and *-5*), were examined. As shown in Table 2A, the M-M group was significantly higher than the other three groups in dacryoadenitis and sialadenitis, and so each of the two loci has an additive effect. Furthermore, the M-H/C group was significantly higher than the C-H/C group in dacryoadenitis and the M-C group was significantly higher than the C-C group in sialadenitis, so *Adacm1* and *Asm3* were hierarchical against *Adacm2* and *Asm5*, respectively.

Next, the interactions of *Adacm3* and the other two loci, *Adacm1* and *-2*, were examined. As shown in Table 2B, there was no significant additive effect, which indicates that *Adacm1* and *-2* have a significant interaction, but *Adacm3* is independent from these two loci.

DISCUSSION

The completion of the human and mouse genome projects has allowed genetic analysis to become a standard approach for identifying alleles for susceptibility to various diseases with multiple phenotypes.[3,2] A cumulative effect of such susceptibility genes resulting from genome crossing may be responsible for the diversity of pathologic manifestations of diseases. In this study, we analyzed the mode of inheritance of dacryoadenitis and sialadenitis in MRL/lpr mice, a mouse model of

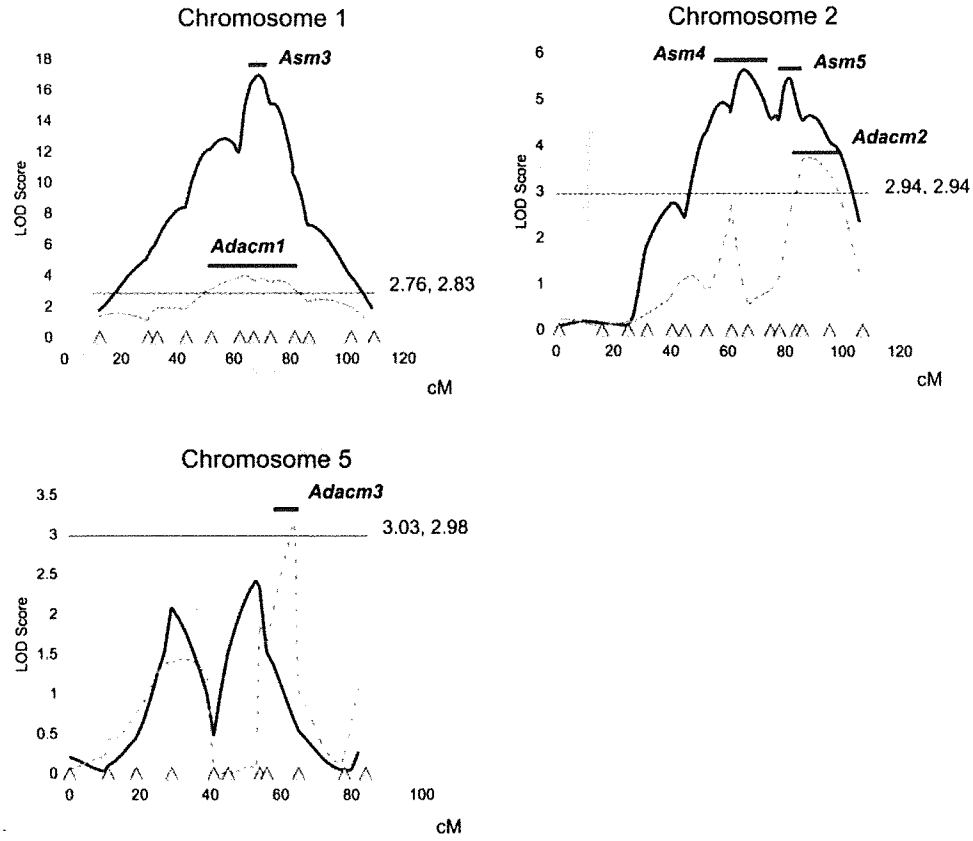

FIGURE 5. Plots of the LOD scores for QTLs that control lacrimal and submandibular lesions in MCF2 progeny. Indexes for chromosomes with significant linkages for dacryoadenitis (chromosome 1, 2, and 5) and sialadenitis (chromosomes 1 and 2) are shown. Indexes for composite interval mapping for dacryoadenitis (*dotted line*) and sialadenitis (*solid line*) are shown in the highest mode for the LOD score on each chromosome (a free mode for all chromosomes). *Horizontal lines* and their values (dacryoadenitis and sialadenitis index, respectively) show the thresholds of significance levels ($\alpha = 0.01$), with the *dotted line* representing the dacryoadenitis index and the *solid line* representing the sialadenitis index, all obtained by analyzing 10,000 random shuffling permutations of the actual data. *Triangles* on the *x*-axis indicate the data for the following microsatellite markers (positions based on information from the Mouse Genome Informatics maintained by The Jackson Laboratory, Bar Harbor, ME; online at http://www.informatics.jax.org) for chromosome 1: *D1Mit276*, *D1Mit18*, *D1Mit22*, *D1Mit46*, *D1Mit49*, *D1Mit187*, *D1Mit286*, *D1Mit394*, *D1Mit202*, *D1Mit143*, *D1Mit291*, and *D1Mit293*; for chromosome 2: *D2Mit355*, *D2Mit83*, *D2Mit522*, *D2Mit323*, *D2Mit380*, *D2Mit37*, *D2Mit102*, *D2Mit441*, *D2Mit395*, *D2Mit304*, *D2Mit258*, *D2Mit22*, *D2Mit285*, *D2Mit50*, and *D2Mit200*; and for chromosome 5: *D5Mit145*, *D5Mit74*, *D5Mit149*, *D5Mit233*, *D5Mit134*, *D5Mit259*, *D5Mit23*, *D5Mit115*, *D5Mit136*, *D5Mit33*, and *D5Mit223*. The 95% confidence intervals of the QTL span were calculated according to the LOD drop-off method described by Lander and Botstein[31] and represented as a solid bar for each QTL.

human SS,[10–12,33] since the lacrimal and submandibular glands in MRL/lpr mice are histopathologically characterized by mononuclear cell infiltration consisting of T cells, B cells, dendritic cells, and macrophages, into periductular regions,[34,35] followed by the progressive destruction of ductules and parenchyma, eventually leading to parenchymal atrophy and replacement of the glandular structures by fibrotic scar tissue.[36] As a result, three susceptibility loci were identified that affect the development of dacryoadenitis and sialadenitis in MRL/lpr mice. These loci were independent of the susceptibility loci to other lupus phenotypes such as glomerulonephritis, vasculitis, and arthritis, which have been identified in the backcrosses and intercrosses of MRL/lpr and C3H/lpr mice.[17–21] Inheritance of dacryoadenitis and sialadenitis in MRL/lpr mice was polygenic, partly characterized by an additive effect and was hierarchical. Each of the polygenes only by itself is not remarkably efficient for disease development. It is likely that all these candidate genes are polymorphic genes in the MRL/Mp strain, different from those in the C3H/HeJ strain. These may quantitatively regulate the cascade reactions extending to the development of dacryoadenitis and/or sialadenitis, with a regular variation of the pathologic phenotypes based on their combinations.

To our knowledge, this is the first study in which the susceptibility loci for dacryoadenitis have been examined. For sialadenitis, two susceptibility loci were identified previously: *Asm1* on chromosome 10 and *Asm2* on chromosome 4 in the MRL genetic background.[21] However, in the present study, we did not detect them in the same chromosomal regions. There were several differences between the earlier study and this one in the experimental methods. For example, MRL/lpr × (MRL/lpr × C3H/lpr) F1 (N2 backcross) was evaluated in the earlier study. However, the MCF2 progeny were examined in this study. In addition, an association study was conducted in the earlier study, but QTL was used in the present study. These distinctions may account for the differences in the positions of the susceptibility loci in both studies. Similar results were seen in the past study for sialadenitis.[24] Namely, QTL was performed on the (NOD × C57BL/6(B6)) F2 cross and ((NOD × B6) × NOD) backcross and no common chromosomal region was identified except for that in chromosome 1. It is likely that in an N2 backcross generation, only recessive loci can be detected, but in an F2 cross, all loci with a recessive, dominant, or incomplete dominant (additive) mode of inheritance can be detected. This difference may lead to the result that all susceptibility to sialadenitis in the present study was due to a additive mode of inheritance, whereas all loci in our previous study were recessive. That is, the difference may depend on the mode of inheritance.

In this study, *Adacm1* was located very close to *Asm3*, whereas *Adacm2* was close to *Asm5*. And *Adacm2* and *Asm5* as well as *Adacm1* and *Asm3* were overlapped in confidence intervals as shown in Figure 5. Therefore, the two susceptibility loci to both lesions are a common genetic basis for the development of these two diseases, although the other was independent. In addition, each of the two loci has an additive effect. Therefore, dacryoadenitis and sialadenitis in MRL/lpr are under the control of different susceptibility loci with an allelic combination.

In addition, a similar tendency is shown in human autoimmune diseases in terms of the partial commonality of susceptibility loci. The co-occurrence of autoimmune diseases is a

TABLE 1. Summary of the Susceptibility Loci for Dacryoadenitis and Sialadenitis in MCF2 Progeny

		QTL											
Phenotype	Chromosome	Designation	Map Position (cM)	LOD Score*	P†	Inheritance‡	Confidence Interval (cM)§	Related Marker (Position, cM)‖	Genotype¶	Mice (n)	Index (Mean ± SD)	Comparison#	P**
Dacryoadenitis	1	*Adacm1*	64.1	4.0	0.0002	Additive	51.0	*D1Mit187* (62.0)	M	120	0.66 ± 0.60	M vs. H	0.004
									H	255	0.48 ± 0.52	M vs. C	5×10^{-5}
									C	136	0.37 ± 0.45	H vs. C	0.04
	2	*Adacm2*	88.4	3.7	0.0002	Recessive	17.3	*D2Mit285* (86.0)	M	134	0.65 ± 0.59	M vs. H/C	6×10^{-5}
									H	256	0.44 ± 0.50		
									C	121	0.37 ± 0.45		
	5	*Adacm3*	63.9	3.1	0.03	Recessive	6.8	*D5Mit136* (65.0)	M	120	0.62 ± 0.58	M vs. H/C	4×10^{-5}
									H	292	0.47 ± 0.53		
									C	99	0.41 ± 0.45		
Sialadenitis	1	*Asm3*	69.0	16.8	3×10^{-17}	Additive	6.2	*D1Mit286* (67.0)	M	126	0.66 ± 0.41	M vs. H	2×10^{-7}
									H	260	0.45 ± 0.34	M vs. C	3×10^{-18}
									C	130	0.26 ± 0.27	H vs. C	3×10^{-8}
	2	*Asm4*	65.3	5.6	2×10^{-6}	Additive	18.6	*D2Mit395* (66.9)	M	141	0.56 ± 0.41	M vs. H	0.008
									H	259	0.45 ± 0.36	M vs C	1×10^{-7}
									C	116	0.31 ± 0.30	H vs C	0.0002
	2	*Asm5*	82.1	5.4	2×10^{-5}	Additive	8.0	*D2Mit22* (84.0)	M	134	0.57 ± 0.41	M vs. H	0.0007
									H	261	0.44 ± 0.36	M vs. C	1×10^{-7}
									C	121	0.34 ± 0.32	H vs. C	0.02

* Determined with WinQTL Cartographer ver 2.5 by composite interval mapping (model 6). Genome-wide significance levels were determined after 10,000 permutations.

† Nonparametric *P* (Kruskall-Wallis test).

‡ Model of inheritance determined with WinQTL Cartographer ver 2.5.

§ 95% confidence intervals of the QTL span were calculated according to the LOD drop-off method described by Lander and Botstein.[31]

‖ Closest marker to the QTL. Map position of the marker was based on the Mouse Genome Informatics (MGI) database.

¶ MRL/MRL and C3H/C3H homozygotes and MRL/C3H heterozygotes were designated M, C, and H, respectively.

An additive mode of inheritance disclosed a complex pattern of interaction, and so all combinations of possible genotypes were considered. H and C genotypes at the *D2Mit285* and *D5Mit136* markers, which were a recessive mode of inheritance, were grouped, respectively. Then, the group of M genotype and the group of H and C genotypes were analyzed.

** Nonparametric *P* (Mann-Whitney *U* test).

TABLE 2. Interactions among Each of the Two Loci for Dacryoadenitis and Sialadenitis in MCF2 Progeny

A. Interactions among Each of the Two Loci Located on Chromosome 1 and 2

Phenotype	Genotype of the Marker*		Mice (*n*)	Index (Mean ± SD)	P†
Dacryoadenitis	*D1Mit187* (*Adacm1*)	*D2Mit285* (*Adacm2*)			
	M	M	32	(0.86 ± 0.63)	‡, §, ‖
	M	H/C	88	(0.58 ± 0.57)	‡
	C	M	35	(0.42 ± 0.47)	
	C	H/C	101	(0.36 ± 0.45)	
Sialadenitis	*D1Mit286* (*Asm3*)	*D2Mit22* (*Asm5*)			
	M	M	29	(0.85 ± 0.45)	§, ‖, ‖
	M	C	33	(0.55 ± 0.32)	‖
	C	M	32	(0.32 ± 0.27)	‡
	C	C	30	(0.11 ± 0.18)	

B. Interactions of *Adacm3* and the Other Two Loci

Phenotype	Genotype of the Marker*		Mice (*n*)	Index (Mean ± SD)	P†
Dacryoadenitis	*D1Mit187* (*Adacm1*)	*D5Mit136* (*Adacm3*)			
	M	M	28	(0.83 ± 0.64)	‖
	M	H/C	92	(0.60 ± 0.58)	
	C	M	38	(0.50 ± 0.56)	
	C	H/C	98	(0.32 ± 0.40)	
Dacryoadenitis	*D2Mit285* (*Adacm2*)	*D5Mit136* (*Adacm3*)			
	M	M	38	(0.77 ± 0.57)	‖
	M	H/C	96	(0.60 ± 0.59)	§
	H/C	M	82	(0.55 ± 0.57)	
	H/C	H/C	295	(0.41 ± 0.47)	

* Genotype of the marker closest to the QTL was presented. MRL/MRL and C3H/C3H homozygotes and MRL/C3H heterozygotes were designated M, C and H, respectively.

† A comparison of the means was performed using the Tukey-Kramer test. ‡ $P < 0.05$; § $P < 0.01$; ‖ $P < 0.001$.

common phenomenon. Monozygotic twins develop autoimmune disease, such as rheumatoid arthritis and systemic lupus erythematosus,[37,38] with a high concordance rate. As a result, genetic predisposition is a dominant factor in the development of autoimmune disease. Association and linkage studies of autoimmune diseases have been conducted in different populations and have demonstrated that several susceptibility loci overlap and the genetic factor consists of two types: one is common to many autoimmune diseases, and the other is specific to a given disorder.[39]

In the present study, the common features for both lesions demonstrated that the susceptibility locus involving *Adacm1* and *Asm3* on chromosome 1 had the highest LOD score among each of the three loci (Table 1). Furthermore, *Adacm1* and *Asm3* on chromosome 1 were hierarchical against *Adacm2* and *Asm5* on chromosome 2, respectively (Table 2). Therefore, the locus on chromosome 1 is most important for development of both lesions, at least in the MRL/lpr allele. This locus was also seen as one with a suggestive linkage to sialadenitis in MRL/lpr × MCF1 backcross.[21] Moreover, a susceptibility locus to sialadenitis on chromosome 1 was also detected in a (NOD × B6) F2 cross, a (NOD × NZW) F2 cross, and a ((NOD × B6) × NOD) backcross.[24] Therefore, this chromosomal region has a significant role, common to sialadenitis and dacryoadenitis.

In contrast, *Adacm3* on chromosome 5 was independent from the other two susceptibility loci to dacryoadenitis. Dacryoadenitis and sialadenitis were observed with varied severity in the MCF2 intercross, but the association of the two lesions was weak (Fig. 4), thus suggesting that the two phenotypes could be separated in an MCF2 intercross. In fact, as a result of the QTL analysis of MCF2, *Adacm3* had no association with either *Adacm1* or *-2* (Table 2). These data suggest that *Adacm3* may be associated with a specific mechanism in the development of dacryoadenitis.

At the region with the highest peak of *Adacm3* there were seven genes according to MGI; *Evi25* (ecotropic viral integration site 25), *Lhx5* (LIM homeobox protein 5), *Mvk* (mevalonate kinase), *Selplg* (selectin, platelet ligand), *Tesc* (tescalcin), *Ubc* (ubiquitin C), and *Vps33a* (vacuolar protein sorting 33A) on chromosome 5 (map position 64 cM),[25] some of which may be responsible for inflammation and cell proliferation processes. *Evi25* is an integration site of the murine leukemia retrovirus in murine leukemias.[40] *Lhx5* is a member of the LIM homeobox gene family that encodes a transcription factor[41] and *Mvk* codes for the mevalonate kinase (MK) which is the first enzyme in the isoprenoid biosynthesis pathway and the decrease in MK activity leads to inflammation.[42] *Selplg* codes for the P-selectin glycoprotein ligand-1 (PSGL-1), a mucin-like glycoprotein which is expressed on the surface membrane of all leukocyte that binds to P- and L-selectin and promotes cell adhesion in the inflammatory response associated with leukocyte rolling and extravasation.[43,44] *UbC* is one of two stress-inducible polyubiquitin genes and constitutes an essential source of Ub in maintaining cellular Ub during cell proliferation and stress and *Vps33a* is homologous to the yeast vacuolar protein-sorting *vps33* which codes the protein that is required for trafficking newly synthesized proteins from the late Golgi network to the vacuole.[45] Further studies should be performed

to determine any allelic polymorphism in these genes between the two strains, at least in the coding and promoter regions.

A marked sex bias of dacryoadenitis and sialadenitis in the MRL parent was observed in Figure 3. A similar tendency was seen for dacryoadenitis in the MCF2 progeny, that is, females demonstrated higher severity than males. Therefore, QTL analysis was conducted separately in male and female mice. As a result, the similar findings to those of the both sexes were obtained. There was no new locus with a significant linkage on any chromosomes (data not shown).

In conclusion, the present study demonstrated that the development of dacryoadenitis and sialadenitis were under the control of polygenes partly with an additive effect and a hierarchical manner. Furthermore, two susceptibility loci to dacryoadenitis seemed to be common to those to sialadenitis, whereas the other was independent from them. Therefore, dacryoadenitis and sialadenitis in MRL/lpr are considered to be under the control of common and different susceptibility genes, with an allelic combination that leads to regular variations in the clinical phenotypes.

Acknowledgments

The authors thank the medical students of Ehime University; and Aoi Sukeda, Yuko Uenaka, and Mami Kobayashi for technical help with the simple sequence-length polymorphism analysis.

References

1. Fox RI, Robinson CA, Curd JG, Kozin F, Howell FV. Sjögren's syndrome: proposed criteria for classification. *Arthritis Rheum.* 1986;29:577–585.
2. Al-Hashimi I, Khuder S, Haghighat N, Zipp M. Frequency and predictive value of the clinical manifestations in Sjögren's syndrome. *J Oral Pathol Med.* 2001;30:1–6.
3. Vitali C, Bombardieri S, Moutsopoulos HM, et al. Preliminary criteria for the classification of Sjögren's syndrome: results of a prospective concerted action supported by the European Community. *Arthritis Rheum.* 1993;36:340–347.
4. Vissink A, Kalk WW, Mansour K, et al. Comparison of lacrimal and salivary gland involvement in Sjögren's syndrome. *Arch Otolaryngol Head Neck Surg.* 2003;129:966–971.
5. Vitali C, Moutsopoulos HM, Bombardieri S. The European Community Study Group on diagnostic criteria for Sjögren's syndrome: sensitivity and specificity of tests for ocular and oral involvement in Sjögren's syndrome. *Ann Rheum Dis.* 1994;53:637–647.
6. Vitali C, Bombardieri S, Moutsopoulos HM, et al. Assessment of the European classification criteria for Sjögren's syndrome in a series of clinically defined cases: results of a prospective multicentre study. The European Study Group on Diagnostic Criteria for Sjögren's Syndrome. *Ann Rheum Dis.* 1996;55:116–121.
7. Fujibayashi T, Sugai S, Miyasaka N, Hayashi Y, Tsubota K. Revised Japanese criteria for Sjögren's Syndrome (1999): availability and validity. *Mod Rheumatol.* 2004;14:425–434.
8. Murphy ED, Roths JB. Autoimmunity and lymphoproliferation: induction by mutant gene lpr, and acceleration by a male-associated factor in strain BXSB mice. In: Rose NR, Bigazzi PE, Warner NL, eds. *Genetic Control of Autoimmune Disease.* New York: Elsevier North Holland; 1978:207–220.
9. Andrews BS, Eisenberg RA, Theofilopoulos AN, et al. Spontaneous murine lupus-like syndromes: clinical and immunopathological manifestations in several strains. *J Exp Med.* 1978;148:1198–1215.
10. Hang L, Theofilopoulos AN, Dixon FJ. A spontaneous rheumatoid arthritis-like disease in MRL/l mice. *J Exp Med.* 1982;155:1690–1701.
11. Hoffman RW, Alspaugh MA, Waggie KS, Durham JB, Walker SE. Sjögren's syndrome in MRL/l and MRL/n mice. *Arthritis Rheum.* 1984;27:157–165.
12. Jonsson R, Tarkowski A, Bäckman K, Holmdahl R, Klareskog L. Sialadenitis in the MRL-l mouse: morphological and immunohistochemical characterization of resident and infiltrating cells. *Immunology.* 1987;60:611–616.
13. Watanabe-Fukunaga R, Brannan CI, Copeland NG, Jenkins NA, Nagata S. Lymphoproliferation disorder in mice explained by defects in Fas antigen that mediates apoptosis. *Nature.* 1992;356:314–317.
14. Rathmell JC, Cooke MP, Ho WY, et al. CD95 (Fas)-dependent elimination of self-reactive B cells upon interaction with CD4+ T cells. *Nature.* 1995;376:181–184.
15. Ashany D, Song X, Lacy E, Nikolic-Zugic J, Friedman SM, Elkon KB. Th1 CD4+ lymphocytes delete activated macrophages through the Fas/APO-1 antigen pathway. *Proc Natl Acad Sci U S A.* 1995;92:11225–11229.
16. Steinberg AD, Raveché ES, Laskin CA, et al. NIH conference. Systemic lupus erythematosus: insights from animal models. *Ann Intern Med.* 1984;100:714–727.
17. Miyazaki T, Ono M, Qu WM, et al. Implication of allelic polymorphism of osteopontin in the development of lupus nephritis in MRL/lpr mice. *Eur J Immunol.* 2005;35:1510–1520.
18. Kamogawa J, Terada M, Mizuki S, et al. Arthritis in MRL/lpr mice is under the control of multiple gene loci with an allelic combination derived from the original inbred strains. *Arthritis Rheum.* 2002;46:1067–1074.
19. Qu WM, Miyazaki T, Terada M, et al. Genetic dissection of vasculitis in MRL/lpr lupus mice: a novel susceptibility locus involving the CD72c allele. *Eur J Immunol.* 2000;30:2027–2037.
20. Yamada A, Miyazaki T, Lu LM, et al. Genetic basis of tissue specificity of vasculitis in MRL/lpr mice. *Arthritis Rheum.* 2003;48:1445–1451.
21. Nishihara M, Terada M, Kamogawa J, et al. Genetic basis of autoimmune sialadenitis in MRL/lpr lupus mice: additive and hierarchical properties of polygenic inheritance. *Arthritis Rheum.* 1999;42:2616–2623.
22. Johansson AC, Nakken B, Sundler M, et al. The genetic control of sialadenitis versus arthritis in a NOD.QxB10.Q F2 cross. *Eur J Immunol.* 2002;32:243–250.
23. Cha S, Nagashima H, Brown VB, Peck AB, Humphreys-Beher MG. Two NOD Idd-associated intervals contribute synergistically to the development of autoimmune exocrinopathy (Sjögren's syndrome) on a healthy murine background. *Arthritis Rheum.* 2002;46:1390–1398.
24. Boulard O, Fluteau G, Eloy L, Damotte D, Bedossa P, Garchon HJ. Genetic analysis of autoimmune sialadenitis in nonobese diabetic mice: a major susceptibility region on chromosome 1. *J Immunol.* 2002;168:4192–4201.
25. Mouse Genome Informatics. T.J.L. Mouse Genome Database (MGD). Bar Harbor, ME: Jackson Laboratory; 2005. Available at http://www.informatics.jax.org/. Accessed November 10, 2008.
26. Lander ES, Green P, Abrahamson J, et al. MAPMAKER: an interactive computer package for constructing primary genetic linkage maps of experimental and natural populations. *Genomics.* 1987;1:174–181.
27. Basten CJ, Weir BS, Zeng ZB. Zmap: a QTL cartographer. In: Smith C, Gavora JS, Benkel B, et al. eds. *Proceedings of the 5th World Congress on Genetics Applied to Livestock Production: Computing Strategies and Software.* Vol. 22. Guelph, Ontario, Canada: 5th World Congress on Genetics Applied to Livestock Production, Organizing Committee; 1994:65–74.
28. Wang S, Basten CJ, Zeng ZB. Windows QTL Cartographer, Version 2.5. Raleigh, NC: Statistical Genetics, North Carolina State University; 2007. Available at http://statgen.ncsu.edu/qtlcart/WQTLCart.htm. Accessed November 10, 2008.
29. Kono DH, Park MS, Theofilopoulos AN. Genetic complementation in female (BXSB × NZW)F2 mice. *J Immunol.* 2003;171:6442–6447.
30. Nettleton D, Doerge RW. Accounting for variability in the use of permutation testing to detect quantitative trait loci. *Biometrics.* 2000;56:52–59.
31. Lander ES, Botstein D. Mapping mendelian factors underlying quantitative traits using RFLP linkage maps. *Genetics.* 1989;121:185–199.

32. Glazier AM, Nadeau JH, Aitman TJ. Finding genes that underlie complex traits. *Science*. 2002;298:2345–2349.
33. Kessler HS. A laboratory model for Sjögren's syndrome. *Am J Pathol*. 1968;52:671–685.
34. Aziz KE, McCluskey PJ, Wakefield D. Characterisation of follicular dendritic cells in labial salivary glands of patients with primary Sjögren syndrome: comparison with tonsillar lymphoid follicles. *Ann Rheum Dis*. 1997;56:140–143.
35. Zeher M, Adány R, Nagy G, Gómez R, Szegedi G. Macrophage containing factor XIII subunit a in salivary glands of patients with Sjögren's syndrome. *J Investig Allergol Clin Immunol*. 1991;1:261–265.
36. Larsson A. Histopathological findings in salivary glands of Sjögren's syndrome. The 100 year Anniversary of Henrik Sjögren. *Hygiena*. 1999;108:10–13.
37. Silman AJ, MacGregor AJ, Thomson W, et al. Twin concordance rates for rheumatoid arthritis: results from a nationwide study. *Br J Rheumatol*. 1993;32:903–907.
38. Winchester R. *Systemic Lupus Erythematosus*. New York: Churchill Living Stone; 1992.
39. Anaya JM, Gómez L, Castiblanco J. Is there a common genetic basis for autoimmune diseases? *Clin Dev Immunol*. 2006;13:185–195.
40. Li J, Shen H, Himmel KL, et al. Leukaemia disease genes: large-scale cloning and pathway predictions. *Nat Genet*. 1999;23:348–353.
41. Sheng HZ, Bertuzzi S, Chiang C, et al. Expression of murine Lhx5 suggests a role in specifying the forebrain. *Dev Dyn*. 1997;208:266–277.
42. Houten SM, Frenkel J, Rijkers GT, Wanders RJ, Kuis W, Waterham HR. Temperature dependence of mutant mevalonate kinase activity as a pathogenic factor in hyper-IgD and periodic fever syndrome. *Hum Mol Genet*. 2002;11:3115–3124.
43. Norman KE, Moore KL, McEver RP, Ley K. Leukocyte rolling in vivo is mediated by P-selectin glycoprotein ligand-1. *Blood*. 1995;86:4417–4421.
44. Sako D, Chang XJ, Barone KM, et al. Expression cloning of a functional glycoprotein ligand for P-selectin. *Cell*. 1993;75:1179–1186.
45. Suzuki T, Oiso N, Gautam R, et al. The mouse organellar biogenesis mutant buff results from a mutation in Vps33a, a homologue of yeast vps33 and Drosophila carnation. *Proc Natl Acad Sci U S A*. 2003;100:1146–1150.

JOURNAL OF OCULAR PHARMACOLOGY AND THERAPEUTICS
Volume 25, Number 6, 2009

DOI: 10.1089/jop.2009.0069

In Vivo and *In Vitro* Investigations of Fungal Keratitis Caused by *Colletotrichum gloeosporioides*

Arisa Mitani,[1] Atsushi Shiraishi,[2] Toshihiko Uno,[1] Hitoshi Miyamoto,[3] Yuko Hara,[1] Masahiko Yamaguchi,[1] and Yuichi Ohashi[1]

Abstract

Purpose: To report a case of fungal keratitis caused by *Colletotrichum gloeosporioides*, which is a rare pathogen in humans.
Methods: An 80-year-old woman developed fungal keratitis after having sustained a traumatic injury during field work. The patient was initially examined by slit-lamp biomicroscopy and the Heidelberg Retina Tomograph II-Rostock Cornea Module (HRT II-RCM). Corneal scrapings were collected and submitted for laboratory investigations.
Results: Many septate, hyphae-like interlocking and branching white lines were observed in the area of the infiltrate by HRT II-RCM. A tentative diagnosis of fungal keratitis was made, and the patient was treated with systemic and topical voriconazole and pimaricin ophthalmic ointment. The infectious focus resolved within 2 weeks, and there were no signs of a recurrence after 3 months of treatment with the antifungal agents. The culture of the corneal scraping grew *C. gloeosporioides*.
Conclusions: HRT II-RCM was useful in detecting filamentous fungi in the cornea. The treatment with voriconazole and pimaricin was effective in the treatment of *C. gloeosporioides* keratitis.

Introduction

FUNGAL KERATITIS REMAINS A difficult and vision-threatening corneal disease. The common etiologic agents of fungal keratitis include *Fusarium solani* and other *Fusarium* species and *Aspergillus* species. The infections are usually caused by a prior ocular injury involving organic materials.

A small number of patients with keratitis cases caused by *Colletotrichum* spp. have been reported, but the precise characteristics of *Colletotrichum* keratitis have still not been determined.[1–4] We present a case of fungal keratitis caused by *Colletotrichum gloeosporioides* that was diagnosed by *in vivo* confocal microscopy and *in vitro* corneal cultures.

Case Report

The patient was an 80-year-old woman who felt dust particles blow into her right eye during farm work on October 13, 2008. She visited a private ophthalmological clinic on October 15, 2008 because her right eye felt irritated. She was treated with topical gatifloxacin and 0.1% betamethasone for 2 days. Because the symptoms did not improve, she was referred to the Ehime University Hospital on October 17, 2008.

On the initial examination, her best corrected visual acuity was 20/2,000 in the right eye and 20/80 in the left eye. Slit-lamp examination of the right eye revealed a grayish, stromal infiltrate with a dry texture and indistinct margins with hypopyon (Fig. 1).

Examination of the cornea with the HRT II-RCM (Heidelberg Engineering, Heidelberg, Germany) showed a mass of interlocking and branching white lines in the area of the infiltrate suggesting filamentous fungus keratitis (Fig. 2). Corneal scrapings were collected, and microscopic examination showed filamentous fungal hyphal fragments. Treatment was begun with oral voriconazole (400 mg/day) p.o., topical 0.1% voriconazole hourly, and pimaricin eye ointment 5 times/day. After beginning the antifungal therapy, the hypopyon disappeared within a few days and the focal infiltrate resolved within 2 weeks. The medications were then tapered over a 3-month period, and the best corrected visual acuity in her right eye improved to 20/25.

[1]Department of Ophthalmology and [2]Department of Ophthalmology and Regenerative Medicine, Ehime University School of Medicine, and [3]Department of Clinical Laboratory, Ehime University Hospital, Shitsukawa, Toon-City, Ehime, Japan.

FIG. 1. Slit-lamp photograph showing a grayish, stromal infiltrate with a dry texture and indistinct margins. An hypopyon can be seen in the anterior chamber.

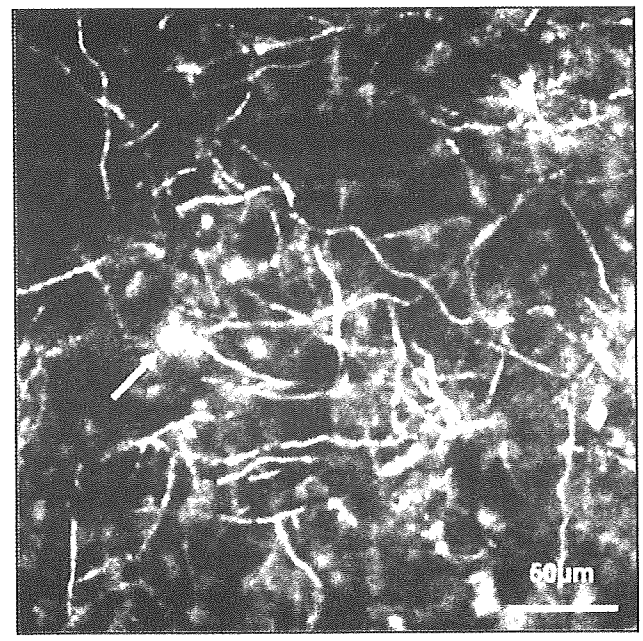

FIG. 2. HRT II-RCM image showing a mass of interlocking and branching white lines and highly reflective spots (*arrow*) which may be appressoria of *Colletotrichum glocosporioides*.

The corneal scrapings grew fungal colonies on Sabouraud dextrose agar, and potato dextrose agar showed brownish-black pigmented colonies (Fig. 3A). Microscopic examination of the culture media showed cylindrical conidia with hyphae (Fig. 3B), and brownish appressoria, features that are characteristic for *C. glocosporioides* (Fig. 3C). The isolate was further

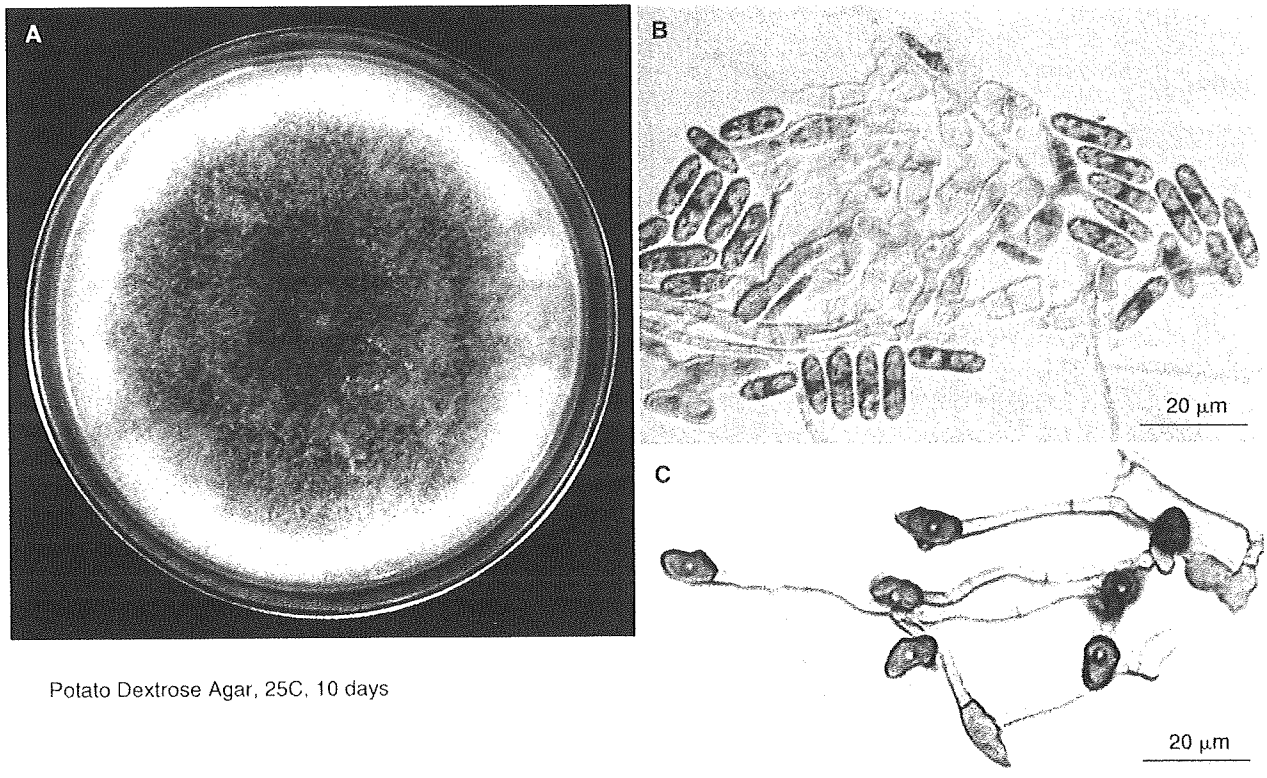

FIG. 3. (**A**) Fungal colonies isolated on potato dextrose agar exhibit brownish-black pigmentation. Microscopic examination of the culture media reveals (**B**) cylindrical conidia with hyphae, and (**C**) brownish appressoria, which are characteristic features of *Colletotrichum glocosporioides*.

TABLE 1. MINIMAL INHIBITORY CONCENTRATION VALUES (MICS) OF DIFFERENT ANTIFUNGAL DRUGS

Drug	*MIC (μg/mL)*
Amphotericin B	0.125
5-Fluconazole	>64
Fluconazole	>64
Intraconazole	0.25
Miconazole	0.5
Micafungin	<0.03
Voriconazole	0.5

confirmed to be *C. gloeosporioides* by DNA sequencing of internal transcribed spacer 1 in rRNA by First Laboratory in Medical Mycology Research Center, Chiba University.

The minimal inhibitory concentrations (MICs) of different antifungal drugs on the fungal isolate are listed in Table 1. This isolate of *C. gloeosporioide* isolated was susceptible to voriconazole.

Discussion

The filamentous fungal plant pathogens belonging to the genus *Colletotrichum* are rare pathogens in humans. The number of reports describing *Colletotrichum* infection in humans is limited; Fernandez and colleagues and Kaliamurthy and colleagues summarized their findings in a series of patients with *Colletotrichum* keratitis, and reported that *Colletotrichum* was the cause of the keratitis in 10 of 360 cases (2.8%) and in 7 of 378 cases (1.9%), respectively.[1,2] They reported that the principal risk factor for *Colletotrichum* keratitis was ocular trauma, followed by the presence of diabetes mellitus and corticosteroid use. Our case occurred after an ocular injury during farm work.

Because there are only a few reports on *Colletotrichum* corneal infection in the literature, the susceptibility of these fungi to antifungals is not clearly established. Fernandez and colleague. reported that some of their isolates from *Colletotrichum* keratitis were susceptible to natamycin and amphotericin B, and that all cases were susceptible to amphotericin B but relatively resistant to natamycin.[1] In our case, the strain isolated was resistant to 5-flucytocine and fluconazole, but susceptible to amphotericin B, itraconazole, miconazole, micafungin, and voriconazole. These results are comparable to the results of the 2 earlier reports that found that *C. gloeosporioide* isolated from subcutaneous hyalohyphomycosis were sensitive to these antifungal drugs.[5,6] Thus, the susceptibility of *Colletotrichum* species appears to be relatively consistent.

We treated our case with pimaricin and voriconazole. Voriconazole is a new, broad-spectrum antifungal drug, and excellent results have been reported following voriconazole treatment in cases of fungal keratitis and endophthalmitis caused by a number of species of fungi.[7–9] Our case is the first to demonstrate that *Colletotrichum* species are susceptible to voriconazole.

We also documented the *in vivo* confocal microscopic appearance of *C. gloeosporioide*. The size of the filaments of the fungus is about 3–5 μm wide and about 100–200 μm long; these are easily recognized by the analytical performance of HRT II-RCM. Our results also support earlier studies that presented the HRT II-RCM images of *F. solani*, *Aspergillus fumigatus*, and *Candida albicans*. These findings demonstrated the usefulness of HRT II-RCM for early diagnosis of fungal keratitis.[10] Although it is difficult to differentiate the different species among filamentous fungi, the highly reflective spots (arrows) were possibly the appressoria of *C. gloeosporioide*. In any case, our results indicate that HRT II-RCM can be a new technique to use for early diagnosis of fungal keratitis.

In conclusion, we report the *in vivo* and *in vitro* investigations of *Colletotrichum* keratitis. More precise microbiological investigations will be required to establish the precise characteristics of *Colletotrichum* species.

Author Disclosure Statement

Financial support: None.

References

1. Fernandez, V., Dursun, D., Miller, D., et al. *Colletotrichum* keratitis. *Am. J. Ophthalmol.* 134:435–438, 2002.
2. Kaliamurthy, J., Kalavathy, C.M., Ramalingam, M.D., et al. Keratitis due to a coelomycetous fungus: case reports and review of the literature. *Cornea.* 23:3–12, 2004.
3. Ritterband, D.C., Shah, M., and Seedor, J.A. *Colletotrichum graminicola*: a new corneal pathogen. *Cornea.* 16:362–364, 1997.
4. Yamamoto, N., Matsumoto, T., and Ishibashi, Y. Fungal keratitis caused by *Colletotrichum gloeosporioides*. *Cornea.* 20:902–903, 2001.
5. Guarro, J., Svidzinski, T.E., Zaror, L., et al. Subcutaneous hyalohyphomycosis caused by *Colletotrichum gloeosporioides*. *J. Clin. Microbiol.* 36:3060–3065, 1998.
6. O'Quinn, R.P., Hoffmann, J.L., and Boyd, A.S. *Colletotrichum* species as emerging opportunistic fungal pathogens: a report of 3 cases of phaeohyphomycosis and review. *J. Am. Acad. Dermatol.* 45:56–61, 2001.
7. Bunya, V.Y., Hammersmith, K.M., Rapuano, C.J., et al. Topical and oral voriconazole in the treatment of fungal keratitis. *Am. J. Ophthalmol.* 143:151–153, 2007.
8. Marangon, F.B., Miller, D., Giaconi, J.A., et al. *In vitro* investigation of voriconazole susceptibility for keratitis and endophthalmitis fungal pathogens. *Am. J. Ophthalmol.* 137:820–825, 2004.
9. Sponsel, W., Chen, N., Dang, D., et al. Topical voriconazole as a novel treatment for fungal keratitis. *Antimicrob. Agents Chemother.* 50:262–268, 2006.
10. Brasnu, E., Bourcier, T., Dupas, B., et al. *In vivo* confocal microscopy in fungal keratitis. *Br. J. Ophthalmol.* 91:588–591, 2007.

Received: June 26, 2009
Accepted: August 28, 2009

Address correspondence to:
Dr. Atsushi Shiraishi
Department of Ophthalmology
Ehime University School of Medicine
Shitsukawa
Toon, Ehime 791-0295
Japan

E-mail: shiraia@m.ehime-u.ac.jp

Rapid detection of *Acanthamoeba* cysts in frozen sections of corneal scrapings with Fungiflora Y

A Shiraishi,[1] T Kobayashi,[1] Y Hara,[2] M Yamaguchi,[2] T Uno,[2] Y Ohashi[2]

See Editorial, p 1555

[1] Department of Ophthalmology and Regenerative Medicine, Ehime University Graduate School of Medicine, Shitsukawa, Toon, Ehime, Japan; [2] Department of Ophthalmology, Ehime University Graduate School of Medicine, Shitsukawa, Toon, Ehime, Japan

Correspondence to: Dr A Shiraishi, Department of Ophthalmology and Regenerative Medicine, Ehime University Graduate School of Medicine, Shitsukawa, Toon, Ehime 791-0295, Japan; shiraia@m.ehime-u.ac.jp

Accepted 14 May 2009

ABSTRACT

Aims: To evaluate the usefulness of serial frozen sections of corneal scrapings stained with Fungiflora Y (FFY) to diagnose *Acanthamoeba* keratitis (AK).

Methods: Eight patients with suspected AK were studied. Serial frozen sections were made from part of the corneal epithelial scrapings and stained with FFY. The remaining corneal epithelial scrapings were submitted for laboratory culture.

Results: The FFY stained frozen sections were completed within an hour, and *Acanthamoeba* cysts were detected under a fluorescence microscope in all eight patients. The same sections were examined with a light microscope, and *Acanthamoeba* cysts were confirmed to be present from their morphological characteristics. Five of the eight patients had positive laboratory cultures for *Acanthamoeba*.

Conclusion: FFY staining of frozen sections of corneal scrapings is a rapid and reliable technique which can be used to make an early diagnosis of AK.

Acanthamoeba keratitis (AK) is an intractable, sight-threatening infection of the cornea and is frequently seen in contact lens wearers. The incidence of AK has increased with increasing numbers of contact lens wearers. The problems with AK include the difficulty in making a correct diagnosis at an early stage, and the lack of specific drugs to treat AK. The early clinical signs of AK are subepithelial infiltrates, pseudodendritic keratitis and radial neurokeratitis, and these lesions often lead to AK being misdiagnosed as herpetic keratitis and or fungal keratitis, resulting in delays in initiating proper treatment. In addition, the ability to grow and identify acantoamoeba in culture is between 30% and 60%,[1 2] and it requires a relatively long time to obtain the results from cultures.

Acanthamoeba cysts can be detected in corneal scraping, impression cytology or biopsies by a variety of staining methods including special stains such as Calcofluor White and Acridine Orange, and also by immunohistochemistry.[3–6] Routine stains such as Haematoxylin and Eosin (H&E), Giemsa, Gram, Periodic Acid Schiff (PAS), and Lactophenol Cotton Blue can also provide a positive identification.[7–10] However, some of the special stains are time-consuming and more complicated, and the routine stains require skilled and experienced examiners to identify the *Acanthamoeba* cysts or trophozoites.

Fungiflora Y (FFY) was originally developed to detect fungi, and it has a specific affinity for chitin and cellulose, which are components of the cell wall of fungi. However, it has been shown that FFY also stains *Acanthamoeba* cysts because cysts also contain cellulose.[11] We present a simple and quick method to detect *Acanthamoeba* cysts in FFY stained frozen sections of corneal scrapings.

MATERIALS AND METHODS

An informed consent for the examination was obtained from all subjects, and this study was approved by Institutional Review Board of Ehime University. The procedures used conformed to the tenets of the Declaration of Helsinki.

Patients

Eight patients (four men, four women) ranging in age from 18 to 37 years with uncontrollable corneal infection were studied. The clinical features of all patients are summarised in table 1. The final diagnosis in all cases was made from epithelial scrapings which were cultured on non-nutrient agar plates with *Escherichia coli* and by FFY staining (Biomate, Tokyo).

Fungiflora Y staining of frozen sections of corneal scrapings

Corneal epithelial scrapings were placed on the bottom of a cryo dish (Shoeiseisaku, Tokyo) and filled with Tissue-Tek OCT Compound (Sakura Finetek, Tokyo). This was followed by freezing with liquid nitrogen or dry ice, and then 10 μm serial frozen sections were cut. The sections were stained with FFY according to the manufacturer's instructions. Briefly, the sections were fixed with 100% ethanol, and a drop of the counterstaining reagent (A solution) was added. After 2 min, the slides were rinsed in running water and stained with the second staining reagent (B solution) for 5 min. The slides were rinsed in running water and observed under a fluorescent microscope at a wavelength of 405 nm.

RESULTS

All eight patients (mean age, 27.8 (SD 6.5) years) were soft contact lens (SCL) wearers and presented with unilateral severe ocular pain and blurred vision. The average duration of the symptoms prior to visiting our hospital was 5–6 weeks with a range of 1–12 weeks. Slit-lamp examination showed a ring infiltrate pattern in one eye (case 8, table 1), dendriform epitheliopathy in five eyes and radial keratoneuritis in seven eyes (fig 1A, table 1). All patients were treated with topical 0.05% chlorhexidine and 1% voriconazole every hour, and corneal epithelial scrapings were taken once or twice per week during the hospitalisation. All patients improved within 2–6 weeks.